**Climate
of the Past**
Discussions

Terrestrial biosphere changes over the last 120 kyr and their impact on ocean δ^{13}C

B. A. A. Hoogakker[1], R. S. Smith[2], J. S. Singarayer[3,4], R. Marchant[5],
I. C. Prentice[6,7], J. R. M. Allen[8], R. S. Anderson[9], S. A. Bhagwat[10], H. Behling[11],
O. Borisova[12], M. Bush[13], A. Correa-Metrio[14], A. de Vernal[15], J. M. Finch[16],
B. Fréchette[15], S. Lozano-Garcia[14], W. D. Gosling[17], W. Granoszewski[36],
E. C. Grimm[18], E. Grüger[19], J. Hanselman[20], S. P. Harrison[21,7], T. R. Hill[15],
B. Huntley[8], G. Jiménez-Moreno[22], P. Kershaw[23], M.-P. Ledru[24], D. Magri[25],
M. McKenzie[26], U. Müller[27,28], T. Nakagawa[29], E. Novenko[12], D. Penny[30],
L. Sadori[25], L. Scott[31], J. Stevenson[32], P. J. Valdes[4], M. Vandergoes[33],
A. Velichko[12], C. Whitlock[34], and C. Tzedakis[35]

[1]Earth Science Department, University of Oxford, South Parks Road, Oxford, OX1 3AN, UK
[2]NCAS-Climate, Department of Meteorology, University of Reading, Reading, RG6 6BB, UK
[3]Department of Meteorology, University of Reading, Reading, RG6 6BB, UK
[4]BRIDGE, School of Geographical Sciences, University of Bristol, University Road, Bristol, BS8 1SS, UK
[5]Environment Department, University of York, Heslington, York, YO10 5DD, UK

Discussion Paper | Discussion Paper | Discussion Paper | Discussion Paper

CPD

11, 1031–1091, 2015

**Terrestrial biosphere
changes and their
impact on ocean
δ^{13}C**

B. A. A. Hoogakker et al.

Title Page

Abstract	Introduction
Conclusions	References
Tables	Figures

◀◀ ▶▶

◀ ▶

Back Close

Full Screen / Esc

Printer-friendly Version

Interactive Discussion

[6]AXA Chair of Biosphere and Climate Impacts, Grand Challenges in Ecosystems and the Environment and Grantham Institute – Climate Change and the Environment, Imperial College London, Department of Life Sciences, Silwood Park Campus, Buckhurst Road, Ascot SL5 7PY, UK

[7]Department of Biological Sciences, Macquarie University, North Ryde, NSW 2109, Australia

[8]Durham University, School of Biological and Biomedical Sciences, Durham, DH1 3LE, UK

[9]School of Earth Sciences and Environmental Sustainability, Box 5964 Northern Arizona University, Flagstaff, Arizona 86011, USA

[10]The Open University, Walton Hall, Milton Keynes MK7 6AA, UK

[11]Department of Palynology and Climate Dynamics, Albrecht-von-Haller Institute for Plant Sciences, University of Göttingen, Untere Karspüle 2, 37073 Göttingen, Germany

[12]Institute of Geography, Russian Academy of Sciences, Staromonetny Lane 19, 119017 Moscow, Russia

[13]Florida Institute of Technology, Biological Sciences, Melbourne, FL 32901, USA

[14]Instituto de Geología, Universidad Nacional Autónoma de México, Cd. Universitaria, 04510, D.F., México

[15]GEOTOP, Université du Québec à Montréal, C.P. 8888, Succursale Centre-Ville, Montréal, QC, H3C 3P8, Canada

[16]School of Agricultural, Earth and Environmental Science, University of KwaZulu-Natal, Private Bag X01, Scottsville, 3209, South Africa

[17]Palaeoecology & Landscape Ecology, IBED, Faculty of Science, University of Amsterdam, P.O. Box 94248, 1090 GE Amsterdam, the Netherlands

[18]Illinois State Museum, Research and Collections Center, 1011 East Ash Street, Springfield, IL 62703, USA

[19]Department of Palynology and Climate Dynamics, Albrecht-von-Haller Institute for Plant Sciences, University of Göttingen, Untere Karspüle 2, 37073 Göttingen, Germany

[20]Westfield State University, Department of Biology, Westfield, MA 01086, USA

[21]Centre for Past Climate Change and School of Archaeology, Geography and Environmental Sciences (SAGES), University of Reading, Whiteknights, RG6 6AH, Reading, UK

[22]Departamento de Estratigrafía y Paleontología, Facultad de Ciencias, Universidad de Granada, Avda. Fuente Nueva S/N, 18002 Granada, España

Title Page

Abstract | Introduction

Conclusions | References

Tables | Figures

◄ | ►

◄ | ►

Back | Close

Full Screen / Esc

Printer-friendly Version

Interactive Discussion

[23]School of Geography and Environmental Science, Monash University, Melbourne, Vic. 3800, Australia

[24]IRD UMR 226 Institut des Sciences de l'Evolution - Montpellier (ISEM) (UM2 CNRS IRD) Place Eugène Bataillon cc 061, 34095 Montpellier CEDEX, France

[25]Sapienza University of Rome, Department of Environmental Biology, 00185 Roma, Italy

[26]Monash University, School of Geography and Environmental Science, Clayton Vic. 3168, Australia

[27]Biodiversity and Climate Research Center (BiK-F), 60325 Frankfurt, Germany

[28]Institute of Geosciences, Goethe-University Frankfurt, 60438 Frankfurt, Germany

[29]Ritsumeikan University, Research Centre for Palaeoclimatology, Shiga 525-8577, Japan

[30]School of Geosciences, The University of Sydney, NSW, 2006, Sydney, Australia

[31]University of the Free State, Faculty of Natural and Agricultural Sciences, Plant Sciences, Bloemfontein 9300, South Africa

[32]Department of Archaeology and Natural History, ANU College of Asia and the Pacific, Australian National University, Canberra, ACT, 0200, Australia

[33]University of Maine, Climate Change Institute, Orono, ME 04469-5790, USA

[34]Montana State University, Department of Earth Sciences, Bozeman, MT 59717-3480, USA

[35]UCL Department of Geography, Gower Street, London, WC1E 6BT, UK

[36]Redakcja serwisu Panstwowego Instytutu Geologicznego, Carpathian Branch, Warsaw, Poland

Correspondence to: B. A. A. Hoogakker (babetteh@earth.ox.ac.uk)

Abstract

A new global synthesis and biomization of long (> 40 kyr) pollen-data records is presented, and used with simulations from the HadCM3 and FAMOUS climate models to analyse the dynamics of the global terrestrial biosphere and carbon storage over the last glacial–interglacial cycle. Global modelled (BIOME4) biome distributions over time generally agree well with those inferred from pollen data. The two climate models show good agreement in global net primary productivity (NPP). NPP is strongly influenced by atmospheric carbon dioxide (CO_2) concentrations through CO_2 fertilization. The combined effects of modelled changes in vegetation and (via a simple model) soil carbon result in a global terrestrial carbon storage at the Last Glacial Maximum that is 210–470 Pg C less than in pre-industrial time. Without the contribution from exposed glacial continental shelves the reduction would be larger, 330–960 Pg C. Other intervals of low terrestrial carbon storage include stadial intervals at 108 and 85 ka BP, and between 60 and 65 ka BP during Marine Isotope Stage 4. Terrestrial carbon storage, determined by the balance of global NPP and decomposition, influences the stable carbon isotope composition (δ^{13}C) of seawater because terrestrial organic carbon is depleted in ^{13}C. Using a simple carbon-isotope mass balance equation we find agreement in trends between modelled ocean δ^{13}C based on modelled land carbon storage, and palaeo-archives of ocean δ^{13}C, confirming that terrestrial carbon storage variations may be important drivers of ocean δ^{13}C changes.

1 Introduction

The terrestrial biosphere (vegetation and soil) is estimated to contain around 2000 Pg C (Prentice et al., 2001) plus a similar quantity stored in peatlands and permafrost (Ciais et al., 2014). Variations in global climate on multi-millennial time scales have caused substantial changes to the terrestrial carbon pools. Quasi-periodic variations in the Earth's orbital configuration (axial tilt with a ~ 41 kyr period, precession with ~ 19

and 23 kyr periods, and eccentricity with ∼ 100 kyr and longer periods) result in small variations in the seasonal and latitudinal distribution of insolation (Berger, 1978). These are amplified by feedback mechanisms such that for the last ∼ 0.8 million years long glacial periods have been punctuated by short interglacials on roughly a 100 kyr cycle. Glacial periods are associated with low atmospheric CO_2 concentrations, lowered sea level and extensive continental ice-sheets; interglacial periods are associated with high (similar to pre-industrial) CO_2 concentrations, high sea level and reduced ice-sheets (Petit et al., 1999; Peltier et al., 2004).

During glacial–interglacial cycles the productivity and size of the terrestrial biosphere are influenced by orbitally forced climatic changes and atmospheric CO_2 concentrations. Expansion of ice-sheets during glacial periods caused a significant loss of land area available for colonization, but this was largely compensated by the exposure of continental shelves due to lower sea level. During the last glacial period the terrestrial biosphere was significantly reduced as forests contracted. It has been estimated that the terrestrial biosphere contained 300 to 700 PgC less carbon during the Last Glacial Maximum (LGM; 21 ka BP) compared with pre-industrial times (Bird et al., 1994; Ciais et al., 2011; Crowley et al., 1995; Duplessy et al., 1988; Gosling and Holden, 2011; Köhler and Fischer, 2004; Prentice et al., 2011). As first noted by Shackleton et al. (1977), the oceanic inventory of ^{13}C is influenced by terrestrial carbon storage because terrestrial organic carbon has a negative signature, due to isotopic discrimination during photosynthesis. Many of the estimates of the reduction in terrestrial carbon storage at the LGM have therefore been based on the observed LGM lowering of deep-ocean $\delta^{13}C$. A reduction in the terrestrial biosphere of this size would have contributed a large amount of CO_2 to the atmosphere, although ocean carbonate compensation would have reduced the expected CO_2 increase to 15 ppm over about 5 to 10 kyr (Sigman and Boyle, 2000).

Many palaeoclimate data and modelling studies have focused on the contrasts between the LGM, the mid-Holocene (6 ka BP) and the pre-industrial period. The BIOME 6000 project (http://www.bridge.bris.ac.uk/resources/Databases/

BIOMES_data) synthesized palaeovegetation records from many sites to provide global datasets for the LGM and mid-Holocene. Data syntheses are valuable in allowing researchers to see the global picture from scattered, individual records, and to enable model-data comparisons. The data can be viewed through the prism of a global, physically based model that allows the point-wise data to be joined together in a coherent way. There are continuous, multi-millennial palaeoenvironmental records that stretch much further back in time than the LGM but they have not previously been brought together in a global synthesis. These records can provide a global picture of transient change in the biosphere and the climate system. Here we have synthesized and biomized (Prentice et al., 1996) a number of these records, providing a new dataset of land biosphere change that covers the last glacial–interglacial cycle.

To improve understanding of land biosphere interactions with the ocean-atmospheric reservoir, we have modelled the terrestrial biosphere for the last 120 kyr (e.g. from the previous – Eemian – interglacial to the pre-industrial period). We present quantitative estimates of changes in the terrestrial biosphere reconstructed from two atmosphere–ocean general circulation model (AOGCM) simulations over the last glacial cycle. We evaluate biome reconstructions based on these climate model outputs using our new biomized synthesis of terrestrial pollen data records, focusing on the pre-industrial period, 6 ka BP (mid-Holocene), 21 ka BP (LGM), 54 ka BP (a relatively warm interval in the last glacial period), 64 ka BP, (a relatively cool interval in the glacial period), 84 ka BP (the early part of the glacial cycle), and 120 ka BP (the Eemian interglacial). We assess the contribution of terrestrial biosphere and carbon storage changes to deep ocean $\delta^{13}C$ over the last 120 kyr by means of a comparison with deep ocean benthic foraminiferal carbon isotope records, representative for the $\delta^{13}C$ of dissolved inorganic carbon of deep water.

2   Methods

2.1   Biomization

Biomization assigns pollen taxa to one or more plant functional types (PFTs) based on basic biological and climatological ranges. The PFTs are assigned to their respective
5 biomes and affinity scores are calculated for each biome (sum of the square roots of pollen percentages contributed by the PFTs in each biome). This method was first developed for Europe (Prentice et al., 1996) and versions of it have been applied to most regions of the world (Jolly et al., 1998; Elenga et al., 2000; Takahara et al., 1999; Tarasov et al., 2000; Thompson and Anderson, 2000; Williams et al., 2000;
10 Pickett et al., 2004; Marchant et al., 2009). We apply these regional PFT schemes (Table 1) to pollen records that generally extend > 40 kyr, assigning the pollen data to megabiomes (tropical forest, warm temperate forest, boreal forest, savannah/dry woodland, grassland/dry shrubland, desert and tundra) as defined by Harrison and Prentice (2003), in order to harmonize regional variations in PFT to biome assignments
15 and to allow globally consistent model-data comparisons.

Table 2 lists the pollen records used. Biomization matrices and megabiome score data can be found in the Supplement. For taxa with no PFT listing, the family PFT was used if part of the regional biomization scheme. Plant taxonomy was checked using www.itis.gov, www.tropicos.org, and the African Pollen Database. Pollen taxa can be
20 assigned to more than one PFT either because they include several species in the genus or family, with different ecologies, or because they comprise species that can adopt different habitats in different environments.

Age models provided with the individual records were used. However, in cases where radiocarbon ages were only provided for specific depths (e.g. Mfabeni, CUX), linear
25 interpolations between dates were used to estimate ages for the remaining depths. Some age models may be less certain, especially at sites which experience variable sedimentation rates and/or erosion. To aid comparison, for several Southern European sites (e.g. Italy and Greece) it has been assumed that vegetation changes occurred

synchronously within the age uncertainties of their respective chronologies, for which there is evidence (e.g. Tzedakis et al., 2004b).

2.2 Model simulations

Global reconstructions of vegetation changes over the last glacial cycle were produced using a vegetation model forced offline using previously published simulations from two AOGCMs. By using two models we could test the robustness of the reconstructions to different climate forcings.

2.2.1 HadCM3

HadCM3 is a general circulation model, consisting of coupled atmospheric model, ocean, and sea ice models (Gordon et al., 2000; Pope et al., 2000). The resolution of the atmospheric model is 2.5° in latitude by 3.75° in longitude by 19 unequally spaced levels in the vertical. The resolution of the ocean is 1.25° by 1.25° with 20 unequally spaced layers in the ocean extending to a depth of 5200 m. The model contains a range of parameterisations, including a detailed radiation scheme that can represent the effects of minor trace gases (Edwards and Slingo, 1996). The land surface scheme used is the Met Office Surface Exchange Scheme 1 (MOSES1; Cox et al., 1999). In this version of the model, interactive vegetation is not included. The ocean model uses the Gent–McWilliams mixing scheme (Gent and McWilliams, 1990), and sea ice is a thermodynamic scheme with parameterisation of ice-drift and leads (Cattle and Crossley, 1995).

Multiple "snap-shot" simulations covering the last 120 kyr have been performed with HadCM3. The boundary conditions and set-up of the original set of simulations have been previously documented in detail in Singarayer and Valdes (2010). The snap-shots were done at intervals of every 1 ka between the pre-industrial (PI) and LGM (21 ka BP), every 2 ka between the LGM and 80 ka BP, and every 4 ka between 80 and 120 ka BP. Boundary conditions are variable between snap-shots but constant for each

simulation. Orbital parameters are taken from Berger and Loutre (1991). Atmospheric concentrations of CO_2 were taken from Vostok (Petit et al., 1999) and CH_4, and N_2O were taken from EPICA (Spahni et al., 2005; Loulergue et al., 2008), all on the EDC3 timescale (Parrenin et al., 2007). The prescription of ice-sheets was achieved with
5 ICE-5G (Peltier (2004) for 0–21 ka BP, and extrapolated beyond 21–120 ka BP using the method described in Eriksson et al. (2012). The simulations were each spun up from the end of previous runs described in Singarayer and Valdes (2010) to adjust to the modified ice-sheet boundary conditions for 470 years. The climate averages described hereafter are of years 470–499. The climate averages were subsequently
10 used to drive the BIOME4 biogeochemistry-biogeography model in order to simulate glacial terrestrial ecosystem changes.

2.2.2 FAMOUS

FAMOUS (Smith, 2012) is an Earth System Model, derived from HadCM3. It is run at approximately half the spatial resolution of HadCM3 to reduce the computational
15 expense associated with atmosphere–ocean GCM simulations without fundamentally sacrificing the range of climate system feedbacks of which it is capable. Pre-industrial control simulations of FAMOUS have both an equilibrium climate and global climate sensitivity similar to that of HadCM3. A suite of transient FAMOUS simulations of the last glacial cycle, conducted with specified atmospheric CO_2, ice-sheets and changes
20 in solar insolation resulting from variation in the Earth's orbit, compare well with the NGRIP, EPICA and MARGO proxy reconstructions of glacial surface temperatures (Smith and Gregory, 2012). Although of a lower spatial resolution than HadCM3, these FAMOUS simulations have the benefit of being transient, and representing low-frequency variability within the climate system, as well as using more physically justified
25 ice-sheet extents before the LGM. For the present study, we use the most realistically-forced simulation of the Smith and Gregory (2012) suite (experiment ALL-ZH), forced with Northern Hemisphere ice-sheets derived from Zweck and Huybrechts (2005), atmospheric CO_2, CH_4 and N_2O concentrations from EPICA and orbital forcing from

Terrestrial biosphere changes and their impact on ocean $\delta^{13}C$

B. A. A. Hoogakker et al.

Title Page

Abstract | Introduction

Conclusions | References

Tables | Figures

◄ | ►

◄ | ►

Back | Close

Full Screen / Esc

Printer-friendly Version

Interactive Discussion

Berger (1978). To allow the transient experiments to be conducted in a tractable amount of time, these forcings were all "accelerated" by a factor of ten, so that the 120 kyr of climate are simulated in 12 model kyr – this method has been shown to have little effect on the surface climate (Timm and Timmerman, 2007; Ganapolski et al., 2010) although it does distort the response of the deep ocean. In addition, we did not include changes in sea level, Antarctic ice volume, or meltwater from ice-sheets to enable the smooth operation of the transient simulations. The impact on the terrestrial carbon budget of ignoring the continental shelves exposed by lower sea-levels will be discussed later; the latter two approximations are unlikely to have an impact over the timescales considered here. Although within the published capabilities of the model, interactive vegetation was not used during this simulation.

2.2.3 BIOME4

BIOME4 (Kaplan et al., 2003) is a biogeochemistry–biogeography model that predicts the global vegetation distribution based on monthly mean temperature, precipitation and sunshine fraction, as well as information on soil texture, depth and atmospheric CO_2. It derives a seasonal maximum leaf area index that maximises NPP for a given PFT by simulating canopy conductance, photosynthesis, respiration and phenological state. Model gridboxes are then assigned biome types based on a set of rules that use dominant and sub-dominant PFTs, as well as environmental limits. Reconstructions of glacial climate states were obtained by adjusting the HadCM3 and FAMOUS simulations to compensate for their individual pre-industrial climate biases in surface temperature and precipitation on monthly timescales. Climate model anomalies were superimposed on the Leemans and Cramer (1991) observed climatology (Kaplan et al., 2003). These reconstructions were then used to force the BIOME4 model. This process allows us to correct for known errors in the climates of HadCM3 and FAMOUS and produce more accurate results from BIOME4, although the method assumes that the model's modern-day errors are systematically present, unchanged over ice-free regions, throughout the whole glacial cycle. Soil properties on exposed

shelves are extrapolated from the nearest pre-industrial land points. There is no special correction for the input climate model temperatures over this exposed land, which results in a slightly subdued seasonal cycle at these points (due to smaller inter-seasonal variation of ocean temperatures). BIOME4 was forced with appropriate CO_2 levels for each time slice simulation (same as used to force the climate model), derived from the ice core records, as described in Sects. 2.2.1 and 2.2.2. As well as affecting productivity, the lower CO_2 concentrations found during the last glacial favour the growth of plants that use the C_4 photosynthetic pathway (Ehleringer et al., 1997), which can affect the distribution of biomes as well. All other BIOME4 parameters as well as soil characteristics were held constant at pre-industrial values.

3 Results

In this section, the results of both the pollen-based biomization for individual regions and the biome reconstructions based on the GCM climate simulations will be outlined. To limit the length of the paper, only main results are covered; the full synthesis dataset and model-based reconstructions are available from the authors.

3.1 Biomization

This method translates fossil pollen assemblages into a form that allows direct data-model comparison and allows the reconstruction of past vegetation conditions.

3.1.1 North America

Two regional PFT schemes were used for sites from North America: the scheme of Williams et al. (2000) for northern and eastern North America and the scheme of Thompson and Anderson (2000) for the western USA. No weighting was applied to trees and shrub pollen data as proposed by Thompson and Anderson (2000) to be able to reconstruct woodland, forest and desert biomes. All biomization matrices and

B. A. A. Hoogakker et al.

scores for individual sites, as well as explanatory files can be found in the Supplement. The Arctic Baffin Island sites (Amarok and Brother of Fog) have highest affinity scores for tundra during the ice-free Holocene and last interglacial.

At Lake Tulane (Florida) the grassland and dry shrubland biome has the highest affinity scores for the last 52 kyr, apart from two short intervals (∼ 14.5 to 15.5 ka and ∼ 36.5 to 37.5 ka) where warm-temperate forest and temperate forest have highest scores. According to Williams et al. (2000), present day, 6 ka BP, and LGM records of most of Florida and the Southwest of America should be characterized by highest affinity scores for the warm-temperate forest biome (Williams et al., 2000). The discrepancy of our biomization results with those of the regional biomization results of Williams et al. (2000) is due to high percentages of *Quercus*, *Pinus* undiff (both are in the grassland and dry shrubland and warm-temperate forest biomes), and Cyperaceae and Poaceae that contribute to highest affinity scores of the grassland and shrubland biome.

In Northwest America pollen data from San Felipe (16 to 47 ka), Potato Lake (last 35 ka), and Bear Lake (last 150 kyr) all show highest scores for the grassland and dry shrubland biome. Potato Lake is currently situated within a forest (Anderson, 1993). In our biomizations *Pinus* pollen equally contribute to scores of boreal forest, temperate forest, warm-temperate forest and the grassland and dry shrubland biomes. In addition, high contributions of Poaceae occur so that the grassland and dry shrubland biome has highest affinity scores throughout the last 35 kyr. At Carp Lake the Holocene is characterized by alternating highest affinity scores between the temperate forest and grassland and dry shrubland biomes whereas during the glacial the grassland and dry shrubland biome attains highest affinity scores. The age model of Carp Lake suggests this record goes back to the Eemian, and if so, then last interglacial climate was lacking the alternation between the temperate forest and grassland and dry shrubland biomes as was the case during the late Holocene. Recent biomizations at Carp Lake and Bear Lake are similar to modern biome observations (Thompson and Anderson, 2000) and those of the LGM also compare well.

3.1.2 Latin America

The regional biomization scheme of Marchant et al. (2009) was used for Latin American locations. Eleven sites from Central and South America are considered here covering a latitudinal gradient of 49° (from 20 to −29°) and an elevation range of 3900 m (from 110–4010 m a.s.l. (above sea level)) (Table 2). Five of the sites are from relatively low elevations (< 1500 m a.s.l.), from north to south these are: Lago Quexil and Petén-Itzá in Guatamala and Salitre, and Colonia and Cambara in South East Brazil. The high elevation records (> 1500 m a.s.l.), with the exception of the most northerly site in Mexico (Lake Patzcuaro), are distributed along the Andean chain: Ciudad Universitaria X (Colombia), Laguna Junin (Peru), Lake Titicaca (Bolivia/Peru) and Salar de Uyuni (Bolivia).

The five lowland sites indicate the persistence of forest biomes for much of the last 130 kyr (Fig. 2). In Central America the Lago Quexil record stretches back to 36 ka BP and has highest affinity scores for the warm-temperate forest biome during the early Holocene. During glacial times the temperate forest biome dominates, intercalated with mainly the grassland and dry shrubland and desert biomes during the LGM and last deglaciation. At Lago Petén-Itzá (also Guatamala) highest affinity scores for the warm-temperate forest biome are recorded for the last 86 kyr. The Salitre and Colonia records are the only Latin American sites that fall within the tropical forest biome today. The majority of the Salitre record shows high affinities for tropical forest from ~ 64 ka BP to modern; apart from an interval coinciding with the Younger Dryas which displays highest affinity scores for the warm-temperate forest biome. The southern most Brazilian record, at Colonia, has highest affinity scores for tropical forest for the last 40 kyr, except between 28 and 21 ka BP (~ coincident with the LGM) when scores were highest for the warm-temperate forest biome. Between 120 and 40 ka BP highest affinity scores alternate between the tropical forest and warm-temperate forest biome at Colonia. To the south, at Cambara (Brazil), highest affinity scores are found for warm-temperate forest during the Holocene and between 38 and 29 ka BP, whilst during the

Title Page

Abstract	Introduction
Conclusions	References
Tables	Figures

|◄ | ►|

◄ | ►

Back | Close

Full Screen / Esc

Printer-friendly Version

Interactive Discussion

interval in between they alternate between warm temperate forest and grassland and dry shrubland.

Apart from Laguna Junin, higher elevation sites (> 1500 m: Lake Patzcuaro, Titicaca, Uyuni, and CUX) do not show a strong glacial–interglacial cycling in their affinity scores; Mexican site Lake Patzcuaro (2240 m) and Colombian site CUX (2560 m) have highest affinity scores mainly for warm-temperate forest over the last 35 kyr, although they alternate between warm-temperate forest and temperate forest during the Holocene and at CUX also during the LGM. Lake Patzcuaro and CUX biomization results for the Holocene, 6 ka BP and LGM compare well with those derived by Marchant et al. (2009). At Uyuni (3643 m) highest affinity scores are for temperate forest and grassland and dry shrubland between 108 and 18 ka BP. At Titicaca (3810 m) high affinity scores are found for temperate forest over the last 130 kyr, apart from during the previous interglacial (Eemian) when highest affinity scores for the desert biome occur. Finally at Ljunin highest affinity scores alternate between warm-temperate forest and temperate forest during the Holocene and temperate forest and grassland and dry shrubland during the glacial.

3.1.3 Africa

For the biomization of African pollen records the scheme of Elenga et al. (2004) was applied. What is specifically different from Southern European biomizations is that Cyperaceae is not included as this taxon generally occurs in high abundances in association with wetland environments where it represents a local signal (Elenga et al., 2004). It is noted that most African sites are from highland or mountain settings, with the exception of Mfabeni (11 m a.s.l.).

At the mountain site Kashiru swamp in Burundi the Holocene is characterized by an alternation of highest affinity scores for tropical forest, warm temperate forest and the grassland and dry shrubland biomes. During most of the glacial, scores are highest for the grassland and dry shrubland biome, preceded by an interval where warm temperate forest showed highest scores. Highest affinity scores for tropical forest and warm

forest were found during the Holocene at the Rusaka Burundi mountain site, whereas those of the last glacial again had highest scores for grassland and dry shrubland biome. At the Rwanda Kamiranzovy site the grassland and dry shrubland biome displayed highest scores during the last glacial (from ∼ 30 ka BP) and deglaciation,

5 occasionally alternating with the warm temperate forest biome. In Uganda at the low mountain site Albert F (619 m) the Holocene and potentially Bølling Allerød is dominated by highest affinity scores for tropical forest, whereas the Younger Dryas and last glacial show highest affinity scores for the grassland and dry shrubland biome. In the higher-elevation Ugandan mountain site Mubwindi swamp (2150 m), the Holocene

10 pollen record shows alternating highest affinity scores between tropical forest and the grassland and dry shrubland biome, whereas the glacial situation is similar to the Albert F site (e.g. dominated by highest scores for the grassland and dry shrubland biome). In South Africa, the Mfabeni Swamp record shows highest affinity scores for the grassland and dry shrubland biome for the last 46 kyr years occasionally, alternated with the

15 savanna and dry woodland biome, and tropical forest during the late Holocene. At the Deva Deva Swamp in the Uluguru Mountains highest affinity scores are for grassland and dry shrubland for the last ∼ 48 kyr. At Saltpan the grassland and dry shrubland biome dominates throughout the succession, including the Holocene and glacial. At Lake Tritrivakely (Madagascar) the grassland and dry shrubland biome dominates,

20 apart from between 3 and 0.6 ka BP when the tropical forest biome dominates. Our results compare well with those of Elenga et al. (2004) who show a LGM reduction in tropical rainforest and lowering of mountain vegetations zones in major parts of Africa.

3.1.4 Europe

For European pollen records three biomization methods were used that are region

25 specific. For Southern Europe the biomization scheme of Elenga et al. (2004) was used, where Cyperaceae is included in the biomization as it can occur as "upland" species characteristic of tundra. For sites from the Alps the biomization scheme of

Prentice et al. (1992) was used, and for Northern European records the biomization scheme of Tarasov et al. (2000).

In Southern Europe at the four Italian sites (Monticchio, Lago di Vico, Lagaccione and Valle di Castiglione) the Holocene and last interglacial show highest affinity scores for warm temperate forest and temperate forest. During most of the glacial and also cold interglacial substages the grassland and dry shrubland biome has highest affinity scores, whereas during warmer interstadial intervals of the last glacial the temperate forest biome had highest affinity scores again. At Tenaghi Phillipon and Ioannina a similar biome sequence may be observed, with highest affinity scores for temperate forest and warm temperate forest during interglacials. During the last glacial and last interglacial cool substages the grassland and dry shrubland biome showed highest affinity scores at Tenaghi Philippon. At Ioannina the LGM and last glacial cool stadial intervals have highest affinity scores for grassland and dry shrubland, whereas affinity scores of glacial interstadial periods are highest for temperate forest. Our biomization results for Southern European sites agree well with those of Elenga et al. (2004) who also found a shift to dryer grassland and dry shrubland biomes.

All four alpine sites are from altitudes between 570 and 670 m and for all four sites the last interglacial period was characterized by having highest scores for the temperate forest biome. At Füramoos the last glacial (note hiatus between 15 and 41 ka BP) showed highest affinity scores for the tundra biome, whilst during the Holocene the temperate forest biome shows highest affinity scores.

Most Northern European sites are mainly represented for the last interglacial period, apart from Horoszki Duze in Poland. At most sites the temperate forest biome and boreal forest biome show highest affinity scores during the last interglacial (Eemian), whereas cool substages and early glacial (Butovka, Horoszki Duze) show high affinity scores for the grass and dry shrubland biome These results compare well with Prentice et al. (2000), who suggest a southward displacement of the Northern Hemisphere forest biomes and more extensive tundra and steppe like vegetation during the LGM.

3.1.5 Asia

For the higher latitude site Lake Baikal the biomization scheme of Tarasov et al. (2000) was used. For the two Japanese pollen sites we used the biomization scheme of Takahara et al. (1999). At Lake Baikal, during the Eemian the highest affinity scores are for boreal and temperate forest; the penultimate deglaciation and cool substage show highest affinity scores for grassland and dry shrubland, similar to Northern European sites. Pollen taxa such as *Carpinus*, *Pterocarya*, *Tilia cordata* and *Quercus* have probably been redeposited or transported over a large distance; however they all make up less than 1 % of the pollen spectrum and therefore did not influence the biomization much.

At Lake Suigetsu in Japan the warm-temperate forest biome shows highest affinity scores over the last 120 kyr; those of other biomes (including tundra) do show increasing affinity scores during glacial times but never exceeding those of the warm-temperate forest biome. At Lake Biwa the warm-temperate forest biome shows highest affinity scores during interglacial times, whilst in-between they alternate between the warm-temperate forest biome and the temperate forest biome. These results agree well with those of Takahara et al. (1999).

3.1.6 East Asia/Australasia

For East Asian and Australasian sites the scheme of Pickett et al. (2004) was used. In Thailand the Khorat Plateau site shows highest affinity scores for the tropical forest biome over the last ∼ 40 kyr. At New Caledonia's Xero Wapa, the warm-temperate forest and tropical forest biomes show highest affinity scores over the last 127 kyr. In Australia's Caledonian Fen interglacial times (Holocene and previous interglacial) the savanna and dry woodland biome has highest affinity scores. During the glacial the grassland and dry shrubland biome generally shows highest affinity scores, occasionally alternated with highest scores for the savanna and dry woodland biome during the early part of Marine Isotope Stage (MIS) 3 and what would be MIS

Title Page

Abstract	Introduction
Conclusions	References
Tables	Figures

|◄ | ►|
◄ | ►
Back | Close

Full Screen / Esc

Printer-friendly Version

Interactive Discussion

5a (ca. 80–85 ka BP). Over most of the last glacial–interglacial cycle highest affinity scores at Lynch's Crater are for the tropical forest and warm temperate forest biomes with the savannah and dry forest biome important during MIS 4 to 2 and generally having the highest affinity scores between 40 and 7 ka BP, probably the result of increased biomass burning (human activities) causing the replacement of dry rainforest by savannah. In addition, the significance of what is considered to be tundra from MIS 4 is due to an increase in Cyperaceae with the expansion of swamp vegetation over what was previously a lake. At Okarito (New Zealand), the temperate forest biome has highest affinity scores throughout (occasionally alternated with warm-temperate forest), apart from during the LGM and deglaciation (∼ 25 to 14 ka BP), where those of savanna and dry woodland, and grassland and dry shrubland show highest affinity scores. Biomization results for the Australian mainland and Thailand agree well with those obtained by Pickett et al. (2004) for the Holocene and LGM.

3.2 HadCM3/FAMOUS model comparison

Although the source codes of HadCM3 and FAMOUS are very similar, differences in the resolution of the models and the setup of their simulations results in a number of differences in both the climate and the vegetation patterns they produce for the last glacial cycle. Specific regions and times where they disagree on the dominant biome type will be discussed later, but there are a number of features that apply throughout the simulations.

Coupled to BIOME4, both models keep the underlying soil types constant as for the modern throughout the glacial cycle. In terms of the global land carbon budget, the largest difference between the models comes from whether sea-level changes are included or not. HadCM3 allows for the exposure of coastal shelves as sea-level changes through the glacial cycle, with reconstructions based on Peltier and Fairbanks (2006) who used the SPECMAP δ^{18}O record (Martinson et al., 1987) to constrain ice volume/sea level change from the last interglacial to the LGM. FAMOUS, on the other hand, keeps global mean sea level as for the present day. As a consequence

Back | Close

Full Screen / Esc

Printer-friendly Version

Interactive Discussion

B. A. A. Hoogakker et al.

the area of land available to vegetation expands and contracts with falling and rising sea level in HadCM3 but remains unchanged in FAMOUS. Inclusion of changing land exposure with sea level therefore allows for significant additional vegetation changes and represents a potentially major factor in the global carbon budget. This difference will be discussed further later.

Because of its lower resolution, FAMOUS does not represent geographic variation at the same scale as HadCM3. This not only affects the areal extent of individual biomes, but also altitude changes, which can have a significant effect on the local climate and resulting biome affinity.

Full details of the climates produced by FAMOUS and HadCM3 in these simulations can be found in Smith and Gregory (2012) and Singarayer and Valdes (2010). In general, land surfaces in HadCM3 simulations are a degree or so colder than in FAMOUS. This difference in temperature is attributed mainly to differences in surface height and ice-sheet ice extent. FAMOUS model results are also, on average, slightly drier compared with those of HadCM3. This is related to the model resolution, with HadCM3 showing much more regional variation (some areas become wetter and some drier), whilst FAMOUS produces a more spatially uniform drying as the climate cools. A notable exception to this general difference is in northwestern Europe, where FAMOUS more closely reproduces the temperatures reconstructed from Greenland ice-cores (Masson-Delmotte et al., 2005), compared to which the HadCM3 simulations used here have a significant warm bias. Millennial scale cooling events and effects of ice-rafting are not features of our model runs, which present a relatively temporally smoothed simulation of the last glacial cycle.

3.3 Data-model comparison

We present here an overview of the vegetation reconstructions for the glacial cycle produced by the climate anomalies from HadCM3 and FAMOUS. We focus on specific periods, since reviewing every detail present in this comparison is unfeasible. We thus compared the modelled reconstructions with the dominant megabiome derived pollen-

based biomizations and each other, restricting our description of the results to major areas of agreement and disagreement. Maps of the dominant megabiomes produced by BIOME4 using the climate anomalies from HadCM3 and FAMOUS for these periods can be seen in Fig. 2.

The pre-industrial period serves as a test-bed to identify biases inherent in our model setup, before climate anomalies have been added. The 6 ka BP mid-Holocene period represents an orbital and ice-sheet configuration favouring generally warm Northern Hemisphere climate (Berger and Loutre, 1991). The LGM simulation at 21 ka BP is at the height of the last glacial cycle, when ice-sheets were at their fullest extent, orbital insolation seasonality was similar to present and CO_2 was at its lowest concentration ($\sim$ 185 ppm), and the resulting climate was cold and dry in most regions. These three time periods form the basis of the standard PMIP2 simulations and were used in the BIOME 6000 project. The 54 ka BP interval is representative of peak warm conditions during Marine Isotope Stage 3 (MIS 3), where both the model climates and some proxy evidence suggest relatively warm conditions, at least for Europe (Voelker et al., 2002). This period had temporarily higher levels of greenhouse gases, an orbital configuration that favours warmer northern-hemisphere summers, and Northern Hemisphere ice sheet volume roughly half that of the LGM. The time slice 64 ka BP represents MIS 4 when both greenhouse gases and northern-hemisphere insolation were lower, and Northern Hemisphere ice volume was two-thirds higher than at 54 ka BP resulting in significantly cooler global climate. 84 ka BP is representative of stadial conditions of the early part of the glacial (at the end of MIS 5), after both global temperatures and atmospheric concentrations of CO_2 have fallen significantly and the Laurentide ice-sheet has expanded to a significant size but before the Fennoscandian ice-sheet can have a major influence on climate. The 84 ka BP period can be compared with the Eemian (120 ka BP, the earliest climate simulation used here), which represents the end of the last interglacial warmth (MIS 5e), before glacial inception. The Eemian period (120 ka BP) differs from the pre-industrial mainly in insolation. The earlier parts of the Eemian (e.g. 125 ka BP) are often studied due to their additional warmth and

Title Page

Abstract | Introduction

Conclusions | References

Tables | Figures

◄ | ►

◄ | ►

Back | Close

Full Screen / Esc

Printer-friendly Version

Interactive Discussion

sea level compared to the Holocene (Dutton and Lambeck, 2012), but 120 ka BP is the oldest point for which both FAMOUS and HadCM3 climates were available.

3.3.1 Pre-industrial

BIOME4 is forced using anomalies from pre-industrial climate produced by HadCM3 and FAMOUS. Differences between our pre-industrial megabiome reconstructions only arise from the way the pre-industrial climate forcing has been interpolated onto the model grids. Differences between the model- and pollen-based reconstructions for this period highlight biases that are not to do with the climates of HadCM3 and FAMOUS, but are inherent to BIOME4, the pollen-based reconstruction method, or simply the limitations of the models' geographical resolution.

Although few of the long pollen records synthesised in this study extend to the modern period and their geographical coverage is sparse, comparison with previous high-resolution biomizations (see Table 1 for details; these studies include the sites synthesised here amongst many others) show that they are generally representative of the regionally dominant biome. The biomized records of Carp Lake and Lake Tulane in North America are exceptions, showing dry grassland conditions rather than the forests (conifer and warm-mixed, respectively) that are more typical of their regions (Williams et al., 2000).

There is generally very good agreement between the BIOME4 output for this period and the high-resolution biomization studies. A notable exception, common to both models, can be seen in the south-west US being misclassified compared to the regional biomization of Thompson and Anderson (2000).The open conifer woodland they assign to sites in this region appears to be sparsely distributed (their Fig. 2) amongst larger areas likely to favour grassland and desert, and thus may be unrepresentative of areas on the scale of the climate model gridboxes. The limitations of HadCM3 and FAMOUS's spatial resolution appear most evident in South America, where the topographically-influenced mix of forest and grassland biomes found by Marchant et al. (2009) cannot be correctly reproduced, with disagreement at the grid-box scale between FAMOUS

Title Page

Abstract | Introduction

Conclusions | References

Tables | Figures

◄ | ►

◄ | ►

Back | Close

Full Screen / Esc

Printer-friendly Version

Interactive Discussion

and HadCM3. Eurasia is generally well reproduced, although the Asian boreal forest does not extend far enough north, and overruns what should be a broad band of steppe around 50° N on its southern boundary. Australia, with a strong gradient in climate from the coasts to the continental areas also shows the influence of the coarse model resolutions, with the translation to the FAMOUS grid more accurately reproducing the southern woodlands but neither model reproducing the full extent of the desert interior. Both Australian records are from the eastern coastal ranges; there are no long continuous records in the interior because of the very dry conditions. Overall, this comparison gives reasonable support to our working hypothesis that BIOME4, operating on the relatively coarse climate model grids we use here, is capable of producing a realistic reconstruction of global biomes.

3.3.2 6 ka BP mid-Holocene

For both the mid-Holocene and LGM periods, the high resolution biomizations of the BIOME6000 project (see Table 1) provide a better base for comparison of our model results than the relatively sparse, long time-series pollen records synthesised in this study. A common thread in the BIOME 6000 studies is the global similarity between the reconstructions for 6 ka BP and the pre-industrial, and this is, by and large, also the message of our BIOME4 reconstructions using both FAMOUS and HadCM3 climate anomalies. A greening on the northern boundary of the central Africa vegetation band is the most notable difference compared to the pre-industrial in the regional biomizations (Jolly et al., 1998), which is also suggested by the long central African pollen records synthesised here. Both climate model-based reconstructions show grassland on the borders of pre-industrial desert areas in North Africa, although the additional precipitation in both models is too weak, and is held a little too far to the south to "green" the desert more fully. FAMOUS shows a limited reduction in the central African tropical forest area than the HadCM3 based reconstruction, agreeing better with the regional biome reconstructions. Both models predict similar patterns and changes in precipitation for this period, but the magnitude of the rainfall in FAMOUS is

slightly lower. The reduction in forest biomes at the tip of South Africa in the FAMOUS reconstruction has some support from Jolly et al. (1998), although BIOME4 on the FAMOUS grid initially overestimates forest in this area.

The model-based reconstructions show limited changes elsewhere too. In North America, FAMOUS's wetter anomalies produce more woodland in the west compared to the pre-industrial, which HadCM3 does not. This is not a widespread difference shown in the regional biomization, although individual sites do change. Marchant et al. (2009) suggest drier biomes than the pre-industrial for some northern sites in Latin America, agreeing with FAMOUS but not HadCM3. For Eurasia and into China, Prentice (1996), Tarasov et al. (2000) and Yu et al. (2000) all suggest greater areas of warmer forest biomes to the north and west across the whole continent, with less tundra in the north. Neither model-based reconstruction shows these differences, however, with some additional grassland at the expense of forest on the southern boundary in HadCM3, and FAMOUS predicting more tundra in the north. Although both models produce warmer summers for this period, in line with the increased seasonal insolation from the obliquity of the Earth's orbit at this time, the colder winters they also predict for Eurasia skew annual average temperatures to a mild cooling which appears to be preventing the additional forest growth to the north and west seen in the pollen-based reconstructions.

3.3.3   21 ka BP (Last Glacial Maximum)

For the LGM, both models and data-based reconstructions predict a global increase in grasslands at the expense of forest, with more tundra in northern Eurasia and desert area in the tropics than during the Holocene. Along with the cooler, drier climate, lower levels of atmospheric CO_2 also favour larger areas of these biomes. Our long pollen records do not have sufficient spatial coverage to fully describe these differences, showing only smaller areas of forest biomes in southern Europe, central Africa and Australia, but there is again good general agreement between the two different model reconstructions and the regional biomizations of the BIOME6000 project.

The model grids do not seem to have sufficient resolution to reproduce much of the band of tundra directly around the Laurentide ice-sheet, but the forest biomes they show for North America are largely supported by Williams et al. (2000). However, Thompson and Anderson (2000) suggest larger areas of the open-conifer biome in the southwestern US than in the Holocene that the models again do not show. Both models predict a smaller Amazon rainforest area. Marchant et al. (2009) suggest that the Holocene rainforest was preceded by cooler forest biomes, whereas both models produce a climate that favours grasslands. Marchant et al. (2009) also provide evidence for cool, dry grasslands in the south of the continent; FAMOUS follows this climatic trend but suggests desert or tundra conditions, whilst HadCM3 shows a smaller area of the desert biome. For Africa, Elenga et al. (2000) show widespread grassland areas where the Holocene has forest, with which the models agree, and dry woodland in the southeast, with which the models do not agree; they appear to be too cold to retain this biome. Elenga et al. (2000) also shows increased grassland area in southern Europe, which is not strongly indicated by the models having some degree of forest cover here.

The large areas of tundra shown by Tarasov et al. (2000) in northern Eurasia to the east of the Fennoscandian ice-sheet are well reproduced by the models, although HadCM3's slightly wetter conditions produce more of the boreal forest in the centre of the continent. The generally smaller amounts of forest cover in Europe in FAMOUS agree with the distribution of tree populations in Europe at the LGM proposed by Tzedakis et al. (2013) better than those from HadCM3, possibly due to HadCM3's warm bias at the glacial maximum. Both models agree with the smaller areas of tropical forest in China and southeast Asia reconstructed by Yu et al. (2000) and Pickett et al. (2004) compared to the Holocene, but have too much forest area in China compared to the biomization of Yu et al. (2000). Neither model reproduces the reconstructed areas of xerophytic biomes in south Australia, or the tropical forest in the north (Pickett et al., 2004).

3.3.4 54 ka BP (Marine Isotope Stage 3)

There are fewer published biomization results for periods before the LGM, so our model-data comparison is restricted to the biomization results at sites synthesised in this paper. Of these sites, only two sites show a different megabiome affiliation with respect to the LGM: in South America Uyuni shows highest affinity scores for the forest biome, and in Australia, Caledonian Fen shows highest affinity scores for the dry woodland biome (both sites show highest affinity score for grassland during the LGM). Overall, the few sites where data are available show little differences compared with the LGM. This is perhaps a surprise given the evidence that this was a relatively warm interval in the glacial, in Europe at least (Voelker et al., 2002). The similar biome assignments are supported by the model simulations in that, although relatively warm compared to the LGM, the model-based reconstructions for 54 ka BP are similar to LGM biomizations at the pollen sites in the Americas, most of southern Europe (apart from Ioannina where the data show highest affinity scores for temperate forest) and east Africa.

In other parts of the world, the biomes simulated at 54 ka BP by the model do differ from those of the LGM. Both model simulations show increased vegetation in Europe and central Eurasia due to the smaller Fennoscandian ice-sheet as well as reduced desert areas in North Africa and Australia, generally reflecting a warmer and wetter climate under higher CO_2 availability. The models disagree on climates and impact on the vegetation in several areas in this period. These include differences related to prescribed ice-sheets, particularly in North America where the ice-sheet configuration in FAMOUS shows a realistic two-dome pattern. Further afield, HadCM3 model has significantly more tropical rainforest, especially in Latin America, and predicts widespread boreal forest cover right across Eurasia. FAMOUS, however, reproduces a more limited vegetation extent, with more grassland in central Eurasia. The differences in the tropics appear to be linked to a wetter climate in HadCM3, possibly due to a stronger response to precessional forcing, whilst the west and

interior of northern Eurasia is cooler in FAMOUS, with a greater influence from the Fennoscandian ice-sheet.

3.3.5   64 ka BP (Marine Isotope Stage 4)

There are only a few differences between biomized records at the LGM, 54 ka BP, and 64 ka BP (Fig. 2). Apart from one southern European site (Ioannina), which has a highest affiliation with grassland (compared with temperate forest during the LGM), the pollen biome affiliations are much the same as at the LGM for the sites presented here. The two sites in northern Australasia show a highest affiliation with the warm-temperate forest biome during this period, compared with tropical forest at 54 ka BP, however affinity scores between the two types are close, so this is unlikely to be related to different climates. The model-based reconstructions support this as they also do not show major differences at the pollen sites.

Both model-based biome reconstructions are, in general, similar to those reproduced for 54 kyr. The climate of 64 kyr simulated in HadCM3 is cooler and drier than for 54 kyr, producing larger areas of tundra in north and east Eurasia and patchy tropical forests. There is less difference between 64 and 54 kyr in the FAMOUS reconstructions, which simulates a cooler climate at 54 kyr compared to HadCM3, so the FAMOUS and HadCM3 biome reconstructions agree better in this earlier period. North American vegetation distributions primarily differ between the models in this period due to the different configurations of the Laurentide ice-sheet imposed on the models.

3.3.6   84 ka BP (Marine Isotope Stage 5b)

The pollen-based biomization for 84 ka BP clearly reflects the warmer and wetter conditions with more CO_2 available than at 64 ka BP, especially in Europe, with the majority of sites showing highest affinity scores for the temperate forest biomes. Sites in other parts of the world show similar affinity scores to the 64 ka BP timeslice, although they are sparse and it is less clear whether they reflect widespread climatic conditions.

The model-based reconstructions reflect the warmer European climate resulting from the small Fennoscandian ice-sheet, with FAMOUS showing some European forest cover, and HadCM3 extending Eurasian vegetation up to the Arctic coast. The HadCM3-based reconstruction shows more of this vegetation to be grassland rather than forest, probably a result of a slightly cooler climate in the model. Around the southern European pollen sites themselves, however, HadCM3 shows little differences and FAMOUS predicts dry woodlands, perhaps a result of poorly modelled Mediterranean storm-tracks that would bring moisture inland.

Although there are still differences in the configuration of the Laurentide ice-sheet between the models, both now reproduce dry vegetation types in Midwest America and significant boreal forest further north. Both models show significantly smaller desert areas in North Africa and forest in the tropical belt than at 64 ka BP, reflecting significant precipitation and higher CO_2 levels here, although both also show a dry anomaly over Latin America that reduces vegetation, especially in the HadCM3 reconstruction. Because of increased rainfall in Australia, HadCM3 simulations show a smaller desert compared with 54 ka BP.

3.3.7   120 ka BP (last interglacial period, Marine Isotope Stage 5e)

This time-slice represents the previous interglacial, and should have the smallest anomalies from the pre-industrial control climate of the models. The pollen-based biomization shows widespread forest cover for Eurasia, with the only other difference from both the 84 ka BP period and the pre-industrial control being Lake Titicaca, which has the highest affinity toward desert for this period. The affinity scores for temperate forest are almost as high for this site, and neither climate model has the resolution to reproduce the local climate for this altitude well, although both do reflect dry conditions near the coast here, possibly as a result of regional climate feedbacks (Bush et al., 2010).

The models do indeed produce relatively small climate anomalies and vegetation in line with the pre-industrial control and each other. Both models produce widespread

Title Page

Abstract   Introduction

Conclusions   References

Tables   Figures

◄   ►

◄   ►

Back   Close

Full Screen / Esc

Printer-friendly Version

Interactive Discussion

forest cover north of 40N, much as for the pre-industrial climate, although FAMOUS is slightly too wet over North America to produce mid-west grasslands as in HadCM3. Both models increase the extent of their tropical forests, although FAMOUS has a relative dry anomaly over central Africa, with less tropical forest than for the pre-industrial or HadCM3, which once again appears to have a stronger response to precessional forcing.

4 Global terrestrial vegetation changes

The general agreement of the modelling results above across the two climate models and the pollen-based synthesis provides confidence in our global biome reconstructions for the last glacial cycle, although with qualifications as described above. Quantitative estimates of changes in the global terrestrial biosphere and the glacial carbon cycle can thus be drawn from our reconstructions.

4.1 Biome areas

Whilst there is general agreement between the biome reconstructions from the FAMOUS and HadCM3 climate anomalies, there are also areas and periods with significant regional differences. A clearer picture of their overall effect on the global biosphere can be seen by using the global total areas of each megabiome for the two models (Fig. 3). Cooler temperatures, reduced moisture, and lower levels of CO_2 through the glacial result in a general reduction of forest biomes and increases in grassland, desert, and tundra. Lower levels of atmospheric CO_2 also preferentially favour plants using the C4 photosynthetic pathway (Ehleringer et al., 1997), contributing to the expansion of the grassland and desert biomes during the glacial. The changes in atmospheric CO_2 levels through the glacial cycle are common to all the BIOME4 runs, so CO_2 fertilisation effects and C3/C4 competition are not responsible for differences in vegetation response between the FAMOUS-

Terrestrial biosphere changes and their impact on ocean δ^{13}C

B. A. A. Hoogakker et al.

and HadCM3-forced simulation. FAMOUS predicts consistently lower areas of warm-temperate and boreal forest than HadCM3, and higher amounts of grassland and desert. FAMOUS also neglects the additional area of land available to HadCM3 as continental shelves are exposed, although some of this additional land is occupied by the Northern Hemisphere ice-sheets in HadCM3. The global total areas highlight a significant oscillation in the areas of the different megabiomes of $\sim 20\,\mathrm{kyr}$ in length – this is particularly notable between 60 and $120\,\mathrm{ka\,BP}$ in the grassland megabiome and results from the $23\,\mathrm{kyr}$ cycle in the precession of the Earth's orbit. The precession cycle exerts a significant influence on the seasonality of the climate, as noted in tropical precipitation records (e.g. the East Asian monsoon; Wang et al., 2008). Such variations are not explicitly evident in the dominant megabiome types at any of the pollen sites, but the precession oscillation does appear in the individual biome affinity scores of several sites (Fig. 4), lending support to this feature of the model reconstructions.

4.2 Net primary productivity

Net primary productivity (NPP) is the net flux of carbon into green plants (in this case terrestrial plants) due to photosynthesis, after accounting for plant respiration. Global NPP derived from our BIOME4 reconstructions for the PI is ~ 70 to $75\,\mathrm{Pg\,C\,yr}^{-1}$. This is somewhat higher than previously estimated present-day range of 46–$62\,\mathrm{Pg\,C\,yr}^{-1}$ (Tinker and Ineson, 1990; Nemani et al., 2003). Recent estimates using eddy covariance flux data estimate global NPP as $\sim 62\,\mathrm{Pg\,C\,yr}^{-1}$ (assuming 50 % carbon use efficiency to convert from GPP to NPP; Beer et al., 2010).

Some other model estimates for the PI are also lower (e.g. Prentice et al., 2011: $59.2\,\mathrm{Pg\,C\,yr}^{-1}$). As mentioned in Sect. 3.3.1, BIOME4 is driven solely by an observational climate dataset due to the anomaly approach used to reduce the impact of climate model biases (see methods Sect. 2.1.3). Therefore, any overestimate in NPP is not a result of the climate model but possibly due to biases in the vegetation model, and/or biases in the observational climatology used to drive the model, and low spatial resolution used. For example, the lower resolution topography does not

represent mountainous regions such as the Andes well nor its topographically-induced variation in vegetation (see Sect. 3.3.1), which may positively skew NPP values. The model may also overestimate NPP compared to observationally based techniques for the modern or pre-industrial partly because it does not contain any representation of non-climatically induced changes, e.g. cultivation or land degradation.

In the LGM simulations global NPP declines to $\sim 42\,\mathrm{PgC\,yr^{-1}}$ in FAMOUS and $48\,\mathrm{PgC\,yr^{-1}}$ in HadCM3. While these are also higher than some other model-based estimates of $28–40\,\mathrm{PgC\,yr^{-1}}$ (e.g. François et al., 1999; 2002), the relative decrease in the LGM in our models to approximately two-thirds of PI is consistent with several previous studies. A calculation based primarily on isotopic evidence has produced an even lower estimate of LGM NPP of $20 \pm 10\,\mathrm{PgC\,yr^{-1}}$ (Ciais et al., 2011); with LGM primary productivity approximately 50 % lower than their PI estimate.

The PI-LGM difference is greater in FAMOUS than in HadCM3 (Fig. 5a) primarily due to the fact that HadCM3's glacial land area increases as sea-level lowers, enabling additional NPP on continental shelf regions, whereas FAMOUS land area remains the same. This is demonstrated by recalculating global NPP for HadCM3 neglecting exposed shelf regions (HadCM3_NS), which then matches the values from FAMOUS (Fig. 5a, green line). The effect of vegetating continental shelves on global NPP is small in comparison to the overall decrease during the glacial period; NPP reduction at the LGM is 40 % for HadCM3_NS and 35 % for HadCM3_S compared to the PI. Further analysis with HadCM3 suggests that CO_2 fertilization and CO_2 forcing of climate are the main driving forces of the glacial NPP decrease – both of these factors are included in our model setups. By comparison, the impact of large continental ice-sheets reducing the land surface area available for primary production is negligible, as these high-latitude areas only contribute a small fraction of global NPP in any case; if the area covered in ice at the LGM is excluded from NPP calculations of the PI, global NPP only decreases by a maximum of $\sim 5\,\mathrm{PgC\,yr^{-1}}$.

Some differences in the timing of some events between the HadCM3 and FAMOUS-forced runs are apparent, especially in the earlier half of the simulation. These phase

shifts, all of the order of a few thousand years, can largely be ascribed to the multiple snap-shot setup of the HadCM3 run, which only produces simulations at 2 or 4 ka intervals, compared to the 1 ka resolution of the FAMOUS-forced biome reconstruction. Differences in the forcing provided by the ice-sheet reconstructions used in the models, as well as in the strength of their responses to orbital forcing in the early part of the glacial (see Fig. 3) may also play a role.

Both models predict lower NPP during the previous interglacial, the Eemian ($-5\,\mathrm{Pg\,C\,yr^{-1}}$). The first large-scale decrease in NPP occurs during the initial glaciation following the Eemian, estimated at about $10\,\mathrm{Pg\,C\,yr^{-1}}$ (both models). NPP values then go up and down by ~ 2 to $5\,\mathrm{Pg\,C\,yr^{-1}}$ until another large drop of $-10\,\mathrm{Pg\,C\,yr^{-1}}$ (HadCM3_S) to $-20\,\mathrm{Pg\,C\,yr^{-1}}$ (HadCM3-NS, FAMOUS _NS) $\sim 70\,\mathrm{ka\,BP}$, associated with MIS 4. NPP than recovers to similar values as between 105 and $70\,\mathrm{ka\,BP}$ (MIS 5d to 5a) during MIS 3, followed by the final reduction ($-10\,\mathrm{Pg\,C\,yr^{-1}}$) to lowest values during the LGM (Fig. 5).

4.3 Terrestrial carbon storage

Early modelling studies and data-based reconstructions produced a range of 270–1100 PgC decrease in terrestrial carbon storage during the LGM compared with pre-industrial time (see summary table 1 in Kohler and Fischer, 2004). These estimates were based on various techniques including isotopic mass balance based on known marine and atmospheric $\delta^{13}C$ values (Bird et al., 1994), and either data-based or simple model-based reconstructions where constant carbon storage per unit area of each biome was assumed (e.g. Prentice et al., 1993; Crowley, 1995). These early estimates were unreliable, however, because (a) they do not account for variation in carbon storage within biomes and (b) they neglect the substantial influence of atmospheric CO_2 concentration on carbon storage (see Prentice and Harrison, 2009, for a fuller discussion). More recent studies have narrowed the range of LGM terrestrial carbon storage decreases to 300–700 PgC. Prentice et al. (2011) estimated a 550–694 PgC decrease at the LGM using the LPX dynamic vegetation model forced by

four Palaeoclimate Modelling Intercomparison Project Phase II climate model runs for the LGM. Using isotopic and modelling methods Ciais et al. (2011) suggested that only 330 PgC less carbon was stored in the terrestrial biosphere at the LGM than PI Holocene. While this is of the same order as other estimates it represents a reduction of only 10 % from PI. Ciais et al. (2011) also included a large inert carbon pool to represent permafrost and peatland carbon storage (which are not included in most dynamic vegetation models). Their optimization procedure suggested that this inert carbon pool was larger by 700 PgC at the LGM than PI, meaning the reduction in their active terrestrial biosphere was therefore larger than most other studies have suggested, at approximately 1000 PgC.

As BIOME4 does not compute the size of the terrestrial carbon reservoir, here we estimate carbon storage over the last glacial cycle using the method of Wang et al. (2011). Consistent with BIOME4's assumption of steady states for its reconstructed vegetation, this method assumes that the carbon storage for each gridpoint is in balance with the modelled NPP, via turnover times characteristic of the soil and vegetation. Total terrestrial carbon storage is then the sum of vegetation carbon, C_{veg}, and soil carbon, C_{soil} derived using equations 1 and 2 below:

$$C_{veg} = \sum_{biome} NPP_{biome} \cdot \tau^v_{biome} \tag{1}$$

$$C_{soil} = \sum_{biome} NPP_{biome} \cdot \tau^s_{biome} \cdot \exp\left[-k(T - T_{ref})\right] \tag{2}$$

where τ^v_{biome} is the turnover time of vegetation carbon, which is assumed to depend primarily on vegetation type, and is therefore kept constant for each mega-biome. The turnover time of soil is heavily dependent on temperature and therefore τ^s_{biome} is modified by the multiplier $\exp[-k(T - T_{ref})]$, where T is the surface temperature at each grid cell, T_{ref} is the temperature for the PI, and $k = 0.034$. The time constants τ^v_{biome} and τ^s_{biome} were estimated separately for the FAMOUS and HadCM3 biome reconstructions

Title Page

Abstract | Introduction

Conclusions | References

Tables | Figures

|◀ | ▶|

◀ | ▶

Back | Close

Full Screen / Esc

Printer-friendly Version

Interactive Discussion

by dividing modern carbon storage by the model's reconstructed modern NPP, using carbon storage values for each megabiome from Prentice et al. (2001).

The differences in modern NPP by biome between HadCM3 and FAMOUS (related to resolution differences between HadCM3 and FAMOUS) result in differences in $\tau^{\text{v}}_{\text{biome}}$

5 and $\tau^{\text{s}}_{\text{biome}}$ values used to calculate carbon storage, and hence different sensitivities to changes in NPP. During the interglacials FAMOUS and HadCM3 estimate high terrestrial carbon storage: 2100 PgC during the pre-industrial period and 2000 PgC during the last interglacial (Fig. 5b). However, entering the glacial, FAMOUS predicted larger carbon storage decreases than HadCM3. During the LGM, the terrestrial carbon

10 reduction of 800 PgC is nearly twice as large in FAMOUS compared with HadCM3_S (470 PgC). Roughly one third of the difference between FAMOUS and HadCM3 results from the increase in continental shelf area in HadCM3 that are not included in FAMOUS. The other two thirds results from the wetter and warmer climate in glacial HadCM3 than FAMOUS. This enables a greater retention of forest biomes, in particular

15 warm temperate and boreal forest (Figs. 2 and 3).

Both HadCM3 and FAMOUS give Holocene total terrestrial carbon storage estimates similar to previous studies including Ciais et al.'s (2011) estimates for the active land biosphere. The reduction in carbon storage at the LGM compared to pre-industrial time according to HadCM3 is within the range given previously, whereas the estimate from

20 FAMOUS is larger than most estimates, but more similar to Ciais et al.'s estimated (2011) decrease for the active terrestrial biosphere.

Closer examination of the trends during the last glacial cycle reveals that modelled terrestrial carbon storage (Fig. 5b) displays a greater level of periodicity on the ~ 23 kyr time-scale than NPP (Fig. 5a), in both FAMOUS and HadCM3 for the early glacial. The

25 prevalence of a ~ 23 kyr cycle relates to the precession of the Earth's orbit, changing the seasonality of climate. For the biome scores this periodicity is particularly notable between 60 and 120 kaBP (when eccentricity modulation of precession is largest) in the grassland and temperate forest megabiome areas (Fig. 3). The largest impact is from the extent to which Northern Hemisphere mid-latitudes are forested (temperate

forest vs. grassland). This variation at 23 kyr periodicity is more evident in FAMOUS than HadCM3, even though both models drive similar sized periodical changes in megabiome coverage. In HadCM3, slightly wetter glacial conditions result in greater overall forested areas; a decline in temperate and tropical forest is compensated for by an increase in warm-temperate and boreal forest (Fig. 3). FAMOUS, on the other hand, shows declines in all forest types through the glacial. This drives a greater glacial decline in FAMOUS carbon storage, as well as slightly larger precessional variation in carbon storage, because other forest types are not compensating periodicities in grassland variation, as they do in HadCM3.

The first large-scale reduction in terrestrial carbon storage occurs shortly after the previous interglacial, where both models (including HadCM3_S) show a 500 PgC decrease (Fig. 5). Predicted sizes of the terrestrial biosphere then vary around a 1800 PgC mean by about ±100 PgC for HadCM3_S and _NS, whereas FAMOUS shows another large decrease at ∼ 65 ka BP by another 500 PgC, providing terrestrial carbon storage estimates in MIS 4 that are similar to the LGM.

4.4 Implications for ocean carbon

Changes in ocean carbon storage have been calculated here by combining the modelled changes in terrestrial biosphere carbon storage with changes in atmospheric carbon dioxide recorded in ice cores. The decrease in atmospheric carbon between the PI and LGM is approximately 180 PgC (Barnola et al., 1987) which when added to the decrease in terrestrial carbon storage, equates to an increase in total ocean carbon storage of 1050 PgC for FAMOUS and 650 PgC for HadCM3_S.

Globally decreased LGM deep ocean stable carbon isotope ratios (δ^{13}C), as recorded by benthic foraminifera at −0.3 to −0.4 ‰, suggests that global LGM terrestrial carbon storage was decreased by 500 to 700 Pg compared with the PI (assuming vegetation and soil δ^{13}C of −25 ‰) (e.g. Broecker and Peng, 1993; Duplessy et al., 1988; Bird et al., 1996; Kaplan et al., 2002; Beerling et al., 1999). A more recent estimate derived from a compilation of 133 ocean cores is −0.34 ± 0.13 ‰ (Ciais

Terrestrial biosphere changes and their impact on ocean δ^{13}C

B. A. A. Hoogakker et al.

et al., 2011). An ensemble of ocean circulation model simulations suggests a similar decrease of −0.31 ± 0.2 ‰ (Tagliabue et al., 2009).

Using our modelled glacial–interglacial terrestrial carbon storage changes the above approach may be inverted to estimate global ocean $\delta^{13}C$ changes over the same time period. The mass balance approach of Bird et al. (1996) was followed to estimate ocean $\delta^{13}C$ at any point from 120 ka BP to the PI. Using the modelled terrestrial biosphere carbon mass and that of the atmosphere (from the ice core record), contributions to global ocean mass changes were estimated. First, changes in total terrestrial biosphere $\delta^{13}C$ were estimated by multiplying the terrestrial carbon storage calculated at each grid point (described above in Sect. 3.4.3) by the model output $\delta^{13}C$ for each grid cell. These were then averaged to produce a global biosphere $\delta^{13}C$ (Fig. 6a). We then assumed a constant atmospheric $\delta^{13}C$. Ice core records suggest variations between −6.5 to −7 ‰ but the time period covered only extends to the LGM (Leuenberger et al., 1992; Lourantou et al., 2010; Schmitt et al., 2012), so we did not estimate $\delta^{13}C$ values between 22 and 120 ka BP and instead kept all values at −6.5 ‰. Sensitivity tests (not shown) demonstrated that the calculated $\delta^{13}C$ ocean changes would not change significantly whether constant or varying atmospheric $\delta^{13}C$ was used (the maximum difference at LGM was 2 % on total ocean $\delta^{13}C$ depending on whether −6.5 or −7 ‰ was assumed). Combining calculated terrestrial and atmospheric $\delta^{13}C$ and assuming total isotopic mass balance over time, total ocean $\delta^{13}C$ was calculated for the last 120 kyr (Fig. 6b).

The modelled terrestrial biosphere $\delta^{13}C$ (Fig. 6a) displays the largest increase during the LGM when atmospheric CO_2 was at its lowest concentrations, due to changes in C_4 vegetation input (C_4 vegetation discriminates against ^{13}C less than C_3 vegetation when carbon is incorporated by photosynthesis). Consequently, $\delta^{13}C$ increases (becomes less negative) when C_4 vegetation is more prevalent. The differences in biome area between FAMOUS and HadCM3 driven output (Fig. 3), in particular warm temperate and boreal forest coverage, do not result in large differences

in terrestrial biosphere δ^{13}C. The extent of C_4 type vegetation is similar between the models and differences in other biomes have little impact on overall isotopic signature.

The reconstructed total ocean δ^{13}C of the two models mimics the trends in total terrestrial carbon storage; when carbon storage is reduced, ocean δ^{13}C decreases and when carbon storage is increased, ocean δ^{13}C increases (Figs. 5 and 6). The total ocean LGM to PI change in δ^{13}C as estimated using this method is −0.34 ‰ for HadCM3_S and −0.65 ‰ for FAMOUS (Fig. 6b). The additional exposed continental shelf areas available in HadCM3 account for only a small proportion of the difference between the two (compare HadCM3_S and HadCM3_NS in Fig. 6b). Even though FAMOUS and HadCM3 display similar trends in terrestrial biosphere δ^{13}C, the larger decrease in terrestrial carbon from FAMOUS results in almost double the change in ocean δ^{13}C. The predicted PI to LGM decrease in total ocean δ^{13}C from HadCM3 is similar to that inferred e.g. by Ciais et al. (2011) and Tagliabue et al. (2009) whereas FAMOUS seems be outside the range of recent estimates.

Recently compiled deep ocean records of Oliver et al. (2010), covering the last glacial cycle, display similar trends to our modelled ocean δ^{13}C over the entire glacial cycle (Fig. 6b and c). The absolute magnitude of glacial–interglacial variation in HadCM3 is closer to that in the reconstructions, whereas FAMOUS variation is nearly twice the magnitude. However, the temporal variation in FAMOUS has some features that are more similar to the data compilation, such as lighter values in MIS 4 that are similar to the LGM values (Fig. 6b and c). The δ^{13}C excursion of deep Pacific δ^{13}C records ∼ 64 ka BP (coincident with Marine Isotope Stage 4 or the early Wisconsin glacial advance) is as large as, or larger than that of the LGM (Oliver et al., 2010), and is not notable in the HadCM3 derived estimates. The very low deep Pacific values might not be completely due to changes in terrestrial carbon storage and perhaps partly relate to reorganisation of water masses and/or ocean productivity (Kohfeld et al., 2005; Leduc et al., 2010). Most longer benthic foraminiferal δ^{13}C records show even lower values during the penultimate glaciation, as part of a longer timescale trend in increasing ocean δ^{13}C since ca. 250 ka BP (Hoogakker et al., 2006; Piotrowski et al.,

2009; Oliver et al., 2010), which is not captured here. This may be related to longer-term carbon reservoirs changes that may be linked to changes in ocean ventilation and/or productivity (Wang et al., 2001; Hoogakker et al., 2006; Rickaby et al., 2007), not represented in our modelling approach.

While the distribution of $\delta^{13}C$ in oceans is affected by several factors such as reorganisation of water masses (especially in the North Atlantic), ocean productivity and export (Brovkin et al., 2002; Kohfeld and Ridgwell, 2009) and nutrient utilisation, the modelled results presented here suggest that the large-scale trends in ocean $\delta^{13}C$ are dominated by terrestrial carbon storage variation, as Shackleton (1977) first proposed.

5 Conclusions

We have used a new global synthesis and biomization of long pollen records in conjunction with model simulations to analyse the sensitivity of the global terrestrial biosphere to climate change over the last glacial–interglacial cycle. Model output and biomized pollen data generally agree, lending confidence to our global-scale analysis of the carbon cycle derived from the model simulations. We used the models to estimate changes in global terrestrial net primary production and carbon storage. Carbon storage variations have a strong 23 kyr (precessional) cycle in the first half of the glacial cycle in particular. Estimates of global carbon storage by HadCM3 at the LGM are ∼ 470 PgC below modern levels if the contribution of exposed continental shelves and their colonisation are taken into account. Estimates of global carbon storage reduction are significantly greater if continental shelf exposure is not included, with FAMOUS showing the largest changes. Other intervals of significant reductions in terrestrial carbon storage include stadial conditions ∼ 115 and 85 ka BP and between 60 and 65 ka BP during Marine Isotope Stage 4. Comparison of modelled ocean $\delta^{13}C$, using output of HadCM3 and FAMOUS, and compiled palaeo-archives of ocean $\delta^{13}C$ suggest a dominant role of terrestrial carbon storage changes in driving ocean $\delta^{13}C$

changes. Modelled ocean $\delta\,^{13}$C changes derived with FAMOUS are larger because of larger simulated changes in terrestrial carbon storage. The differences in terrestrial carbon storage between the models in turn derive from differences in the variability of ice-sheet prescription (Fig. 3) and regional climate biases, where HadCM3 is generally

5　wetter and slightly warmer in the glacial than FAMOUS, which means productivity and extent of warm temperate and boreal forests does not decrease as it does into the glacial in FAMOUS.

Existing data coverage is still low, and so there are still large areas of uncertainty in our knowledge of the palaeo-Earth system. Better spatial and temporal coverage for all

10　parts of the globe, especially lowland areas, is required, and for this we need data from new sites incorporated into global datasets that are easily accessible by the scientific community.

The synthesised biomized dataset presented in this paper can be downloaded as supplementary material to this paper, or may be obtained by contacting the authors.

15　**The Supplement related to this article is available online at doi:10.5194/cpd-11-1031-2015-supplement.**

References

Allen, J. R. M., Brandt, U., Hubberten, H.-W., Huntley, B., Keller, J., Kraml, M., Mackensen, A., Mingram, J., Negenkamp, J. F. W., Nowaczyk, N. R., Oberhänsli, H., Watts, W. A., Wulf, S.,

and Zolitschka, B.: Rapid environmental changes in southern Europe during the last glacial period, Nature, 400, 740–743, 1999.

Anderson, R. S.: A 35,000 year vegetation and climate history from Potato Lake, Mogollon Rim, Arizona, Quaternary Res., 40, 351–359, 1993.

Barnola, J. M., Raynaud, D., Korotkevich, Y. S., and Lorius, C.: Vostok ice core provides 160,000 year record of atmospheric CO_2, Nature, 329, 408–414, 1987.

Beer, C., Reichstein, M., Tomelleri, E., Ciais, P., Jung, M., Carvalhais, N., Rödenbeck C., Arain, M. A., Baldocchi, D., Bonan, G. B., Bondeau, A., Cescatti, A., Lasslop, G., Lindroth, A., Lomas, M., Luyssaert, S., Margolis, H., Oleson, K. W., Roupsard, O., Veenendaal, E., Viovy, N., Williams, C., Woodward, F., and Papale, D.: Terrestrial gross carbon dioxide uptake: global distribution and covariation with climate, Science, 329, 834–838, 2010.

Beerling, D. J.: New estimates of carbon transfer to terrestrial ecosystems between the last glacial maximum and the Holocene, Terra Nova, 11, 162–167, 1999.

Behling, H., Pillar, V., Orlóci, L., and Bauermann, S. G.: Late Quaternary *Araucaria* forest, grassland (Campos), fire and climate dynamics , studied by high-resolution pollen, charcoal and multivariate analysis of the Cambarára do Sul core in southern Brazil, Palaeogeogr. Palaeoclim. Paleoecol., 203, 277–297, 2004.

Berger, A.: Long-term variations of daily insolation and Quaternary climatic changes, J. Atmos. Sci., 35, 2362–2367, 1978.

Berger, A. and Loutre, M. F.: Insolation values for the climate of the last 10 million years, Quaternary Sci. Rev., 10, 297–317, 1991.

Beuning, K. R. M., Talbot, M., and Kelts, K.: A revised 30,000 year paleoclimatic and paleohydrologic history of Lake Albter, East Africa, Palaeogeogr. Palaeoclim. Paleoecol., 136, 259–279, 1997.

Bird, M., Lloyd, J., and Farquhar, G. D.: Terrestrial carbon storage at the LGM, Nature, 371, 566, 1994.

Bird, M., Lloyd, J., and Farquhar, G. D.: Terrestrial carbon storage from the last glacial maximum to the present, Chemosphere, 33, 1675–1685, 1996.

Bonnefille, R. and Chalié, F.: Pollen-inferred precipitation time series from equatorial mountains, Africa, the last 40 kyr BP, Global Planet. Change, 26, 25–50, 2000.

Borisova, O. K.: Vegetation and climate changes at the Eemian/Weichselian transition: new palynological data from central Russian Plain, Polish Geological Institute Special Papers, 16, 9–17, 2005.

Title Page

Abstract | Introduction

Conclusions | References

Tables | Figures

◄◄ | ►►

◄ | ►

Back | Close

Full Screen / Esc

Printer-friendly Version

Interactive Discussion

Broeker, W. S. and Peng, T.-H.: What caused the glacial to interglacial CO change?, in: The Global Carbon Cycle, edited by: Heimann, M., Springer, Berlin Heidelberg, 95–115, 1993.

Brovkin, V., Bendtsen, J., Claussen, M., Ganopolski, A., Kubatzki, C., Petoukhov, V., and Andreev, A.: Carbon cycle, vegetation, and climate dynamics in the Holocene: experiments with the CLIMBER-2 model, Global Biogeochem. Cy., 16, 1139, doi:10.1029/2001gb001662, 2002.

Bush, M. B., Hanselman, J. A., and Gosling, W. D.: Non-linear climate change and Andean feedbacks: an imminent turning point?, Glob. Change Biol., 16, 3223–3232, 2010.

Cattle, H. and Crossley, J.: Modelling Arctic climate-change, Philos. T. R. Soc. A, 352, 201–213, 1995.

Chepstow-Lusty, A. J., Bush, M. B., Frogley, M. R., Baker, P. A., Fritz, S. C., and Aronson, J.: Vegetation and climate change on the Bolivian Altiplano between 108,000 and 18,000 yr ago, Quaternary Res., 63, 90–98, 2005.

Ciais, P., Tagliabue, A., Cuntz, M., Bopp, L., Scholze, M., Hoffmann, G., Lourantou, A., Harrison, S. P., Prentice, I. C., Kelley, D. I., Koven, C., and Piao, S. L.: Large inert carbon pool in the terrestrial biosphere during the Last Glacial Maximum, Nat. Geosci., 5, 74–79, 2012.

Correa-Metrio, A., Bush, M. B., Cabrera, K. R., Sully, S., Brenner, M., Hodell, D. A., Escobar, J., and Guilderson, T.: Rapid climate change and no-analog vegetation in lowland Central America during the last 86,000 years, Quaternary Sci. Rev., 38, 63–75, 2012.

Cox, P. M., Betts, R. A., Bunton, C. B., Essery, R. L. H., Rowntree, P. R., and Smith, J.: The impact of new land surface physics on the GCM simulation of climate and climate sensitivity, Clim. Dynam., 15, 183–203, 1999.

Crowley, T. J.: Ice age terrestrial carbon changes revisited, Global Biogeochem. Cy., 9, 377–389, 1995.

Duplessy, J. C., Shackleton, N. J., Fairbanks, R. G., Labeyrie, L., Oppo, D., and Kallel, N.: Deepwater source variations during the last climatic cycle and their impact on the global deepwater circulation, Paleoceanography, 3, 343–360, 1988.

Dutton, A. and Lambeck, K.: Ice volume and sea level during the last interglacial, Science, 337, 216–219, 2012.

Edwards, J. M. and Slingo, A.: Studies with a flexible new radiation code.1. Choosing a configuration for a large-scale model, Q. J. Roy. Meteor. Soc., 122, 689–719, 1996.

Title Page

Abstract | Introduction

Conclusions | References

Tables | Figures

|◄ | ►|

◄ | ►

Back | Close

Full Screen / Esc

Printer-friendly Version

Interactive Discussion

Elenga, H., Peyron, O., Bonnefille, R, Jolly, D., Cheddadi, R., Guiot, J., Andrieu, V., Bottema, S., Buchet, G., de Beaulieu, J.-L., Hamilton, A. C., Maley, J., Marchant, R., Perez-Obiol, R., Reille, M., Riollet, G., Scott, L., Straka, H., Taylor, D., Van Campo, E., Vincens, A., Laarif, F., and Jonson, H.: Pollen-based biome reconstruction for Southern Europe and Africa 18,000 yr BP, J. Biogeogr., 27, 621–634, 2004.

Elsig, J., Schmitt, J., Leuenberger, D., Schneider, R., Eyer, M., Leuenberger, M., Joos, F., Fischer, H., and Stocker. T. S.: Stable isotope constraints on Holocene carbon cycle changes from an Antarctic ice Core, Nature, 461, 507–510, 2004.

Eriksson, A., Betti, L., Friend, A. D., Lycett, S. J., Singarayer, J. S., Von Cramon, N., Valdes, P. J., Balloux, F., and Manica, A.: Late Pleistocene climate change and the global expansion of anatomically modern humans, P. Natl. Acad. Sci. USA, 109, 16089–16094, 2012.

Finch, J. M. and Hill, T. R.: A late Quaternary pollen sequence from Mfabeni Peatland, South Africa: reconstructing forest history in Maputaland, Quaternary Res., 70, 442–450, 2008.

Finch, J., Leng, M. J., and Marchant, R.: Late Quaternary vegetation dynamics in a biodiversity hotspot, the Uluguru Mountains of Tanzania, Quaternary Res., 72, 111–122, 2009.

François L. M., Goddérisa, Y., Warnanta, P., Ramstein, G., de Noblet, N., and Lorenzc, S.: Carbon stocks and isotopic budgets of the terrestrial biosphere at mid-Holocene and last glacial maximum times, Chem. Geol., 159, 163–189, 1999.

François, L., Faure, H., and Probst, J.-L.: The global carbon cycle and its changes over glacial–interglacial cycles, Global Planet. Change, 33, vii–viii, 2002.

Fréchette, B., Wolfe, A. P., Miller, G. H., Richard, P. J. H., and de Vernal, A.: Vegetation and climate of the last interglacial on Baffin Island, Arctic Canada, Palaeogeogr. Palaeoclim. Paleoecol., 236, 91–106, 2006.

Fritz, S. C., Baker, P. A., Seltzer, G. O., Ballantyne, A., Tapia, P. M., Cheng, H., and Edwards, R. L.: Quaternary glaciation and hydrologic variation in the South American tropics as reconstructed from the Lake Titicaca drilling project, Quaternary Res., 68, 410–420, 2007.

Ganopolski, A., Calov, R., and Claussen, M.: Simulation of the last glacial cycle with a coupled climate ice-sheet model of intermediate complexity, Clim. Past, 6, 229–244, doi:10.5194/cp-6-229-2010, 2010.

Gasse, F. and Van Campo, E.: A 40,000 yr pollen and diatom record from Lake Tritivakely, Madagascar, in the Southern Tropics, Quaternary Res., 49, 299–311, 1998.

Title Page

Abstract | Introduction

Conclusions | References

Tables | Figures

◄ | ►

◄ | ►

Back | Close

Full Screen / Esc

Printer-friendly Version

Interactive Discussion

Gent, P. R. and McWilliams, J. C.: Isopycnal mixing in ocean circulation models, J. Phys. Oceanogr., 20, 150–155, 1990.

Gordon, C., Cooper, C., Senior, C. A., Banks, H., Gregory, J. M., Johns, T. C., Mitchell, J. F. B., and Wood, R. A.: The simulation of SST, sea ice extents and ocean heat transports in a version of the Hadley Centre coupled model without flux adjustments, Clim. Dynam., 16, 147–168, 2000.

Gosling, W. D. and Holden, P. D.: Precessional forcing of tropical vegetation carbon storage, J. Quaternary Sci., 26, 463–467, 2011.

Gosling, W. D., Bush, M. B., Hanselman, J. A., and Chepstow-Lusty, A.: Glacial–interglacial changes in moisture balance and the impact of vegetation in the Southern Hemisphere tropical Andes (Bolivia/Peru), Palaeogeogr. Palaeoclim. Paleoecol., 259, 35–50, 2008.

Grichuk, V. P., Zelikson, E. M., and Nosov, A. A.: New data on the interglacial deposits near Il'inskoye on the Yakhroma River, Bulleten' Komissii po Izucheniyu Chetvertichnogo Perioda, 52, 150–156, 1983.

Grimm, E. C., Watts, W. A., Jacobson, G. L., Hansen, B. C. S., Almquist, H. R., and Dieffenbacher-Krall, A. C.: Evidence for warm wet Heinrich events in Florida, Quaternary Sci. Rev., 25, 2197–2211, 2006.

Grüger, E.: Spätriß, Riß/Würm und Frühwürm am Samerberg in Oberbayern – ein vegetationsgeschichtlicher Beitrag zur Gliederung des Jungpleistozäns, Geol. Bavarica, 80, 5–64, 1979a.

Grüger, E.: Die Seeablagerungen vom Samerberg/Obb. und ihre Stellung im Jungpleistozan, Eiszeitalter und Gegenwart, 29, 23–34, 1979b.

Grüger, E. and Schreiner, A.: Riß/Würm- und würmzeitliche Ablagerungen im Wurzacher Becken (Rheingletschergebiet), Neues Jahrbuch für Geologie und Paläontologie, Abhandlungen, 189, 81–117, 1993.

Hanselman, J. A., Bush, M. B., Gosling, W. D., Collins, A., Knox, C., Baker, P. A., and Fritz, S. C.: A 370,000 year record of vegetation and fire history around Lake Titicaca (Bolivia/Peru), Palaeogeogr. Palaeoclim. Paleoecol., 305, 201–214, 2011.

Hansen, B. C. W., Wright, H. E. Jr., and Bradbury, J. P.: Pollen studies in the Junin area, central Peruvian Andes, Geol. Soc. Am. Bull., 95, 1454–1465, 1984.

Harrison, S. P. and Prentice, C. I.: Glimate and CO_2 controls on global vegetation distribution at the last glacial maximum: analysis based on palaeovegetation data, biome modelling and palaeoclimate simulations, Glob. Change Biol., 9, 983–1004, 2003.

Terrestrial biosphere changes and their impact on ocean δ^{13}C

B. A. A. Hoogakker et al.

Title Page

Abstract	Introduction
Conclusions	References
Tables	Figures

Back | Close

Full Screen / Esc

Hoogakker, B. A. A., Rohling, E. J., Palmer, M. R., Tyrrell, T., and Rothwell, R. G.: Underlying causes for long-term global ocean $\delta^{13}C$ fluctuations over the last 1.20 Myr, Earth Planet. Sc. Lett., 248, 15–29, 2006.

Indermühle, A., Stocker, T. F., Joos, F., Fischer, H., Smith, H. J., Wahlen, M., Deck, B., Mastroianni, D., Tschumi, J., Blunier, T., Meyer, R., and Stauffer, B.: Holocene carbon-cycle dynamics based on CO_2 trapped in ice at Taylor Dome, Antarctica, Nature, 398, 121–126, 1999.

Jiménez-Moreno, G., Anderson, R. S., and Fawcett, P. J.: Orbital- and milennial-scale vegetation and climate changes of the past 225 ka from Bear Lake, Utah-Idaho (USA), Quaternary Sci. Rev., 26, 1713–1724, 2007.

Jolly, D., Prentice, C., Bonnefille, R., Ballouche, A., Bengo, M., Brenac, P., Buchet, G., Burney, D., Cazet, J. P., Cheddadi, R., Edorh, T., Elenga, H., Elmoutaki, S., Guiot, J., Laarif, F., Lamb, H., Lezine, A. M., Maley, J., Mbenza, M., Peyron, O., Reille, M., Raynaud-Farrera, I., Riollet, G., Ritchi, J. C., Roche, E., Scott, L., Ssemmanda, I., Straka, H., Umer, M., van Campo, E., Vilimumbalo, S., Vincens, A., and Waller, M.: Biome reconstruction from pollen and plant macrofossil data for Africa and the Arabian peninsula at 0 and 6000 Years, J. Biogeogr., 25, 1007–1027, 1998.

Joos, F., Gerber, S., Prentice, I. C., Otto-Bliesner, B., and Valdes, P.: Transient simulations of Holocene atmospheric carbon dioxide and terrestrial carbon since the Last Glacial Maximum, Global Biogeochem. Cy., 18, GB2002, doi:10.1029/2003GB002156, 2004.

Kaplan, J. O., Prentice, I. C., and Buchmann, N.: The stable carbon isotope composition of the terrestrial biosphere: modeling at scales from the leaf to the globe, Global Biogeochem. Cy., 16, 1060, doi:10.1029/2001GB001403, 2002.

Kaplan, J. O., Bigelow, N. H., Bartlein, P. J., Christensen, T. R., Cramer, W., Harrison, S. P., Matveyeva, N. V., McGuire, A. D., Murray, D. F., Prentice, I. C., Razzhivin, V. Y., Smith, B., Walker, D. A., Anderson, P. M., Andreev, A. A., Brubaker, L. B., Edwards, M. E., Lozhkin, A. V., and Ritchie, J.: Climate change and Arctic ecosystems II: modeling, palaeodata-model comparisons, and future projections, J. Geophys. Res., 108, 8171, doi:10.1029/2002JD002559, 2003.

Kershaw, P.: Climate change and Aboriginal burning in north-east Australia during the last two glacial/interglacial cycles, Nature, 322, 47–49, 1986.

Kershaw, A. P., McKenzie, G.M, Porch, N., Roberts, R. G., Brown, J., Heijnis, H., Orr, L. M., Jacobsen, G., and Newall, P. R.: A high resolution record of vegetation and climate through

the last glacial cycle from Caledonia Fen, south-eastern highlands of Australia, J. Quaternary Sci., 22, 481–500, 2007.

Kohfeld, K. E. and Ridgwell, A.: Glacial–interglacial variability in atmospheric CO_2, in: Surface Ocean–Lower Atmospheres Processes, edited by: Le Quéré, C. and Saltzman, E. S., AGU Geoph. Monog. Series, Vol. 187, American Geophysical Union (AGU), Washington D.C., 350 pp., 2009.

Kohfeld, K. E., Le Quéré, C., Harrison, S. P., and Anderson, R. F.: Role of marine biology in glacial–interglacial CO_2 cycles, Science, 308, 74–78, 2005.

Köhler, P. and Fischer, H.: Simulating changes in the terrestrial biosphere during the last glacial/interglacial transition, Global Planet. Change, 43, 33–55, 2004.

Ledru, M.-P., Behling, H., Fournier, M. L., Martin, L., and Servant, M.: Localisation de la fôret d'Acaucaria du Brazil au cours de l'Holocène. Implications paleoclimatiques, C. R. Acad. Sci. Paris, 317, 517–521, 1994.

Ledru, M.-P., Soares Braga, P. I., Soubies, F., Fournier, M. L., Martin, L., Suguio, K., and Turcq, B.: The last 50,000 years in the Neotropics (southern Brazil): evolution of vegetation and climate, Palaeogeogr. Palaeoclim. Paleoecol., 123, 239–257, 1996.

Ledru, M.-P., Mourguiart, P., and Riccomini, C.: Related changes in biodiversity, insolation and climate in the Atlantic rainforest since the last interglacial, Palaeogeogr. Palaeoclim. Paleoecol., 271, 140–152, 2009.

Leduc, G., Vidal, L., Tachikawa, A., and Bard, E.: Changes in Eastern Pacific Ocean ventilation at intermediate depth over the last 150 kyr BP, Paleoceanography, 298, 217–228, 2010.

Leemans, R. and Cramer, W. P.: The IIASA Database for Mean Monthly Values of Temperature, Precipitation, and Cloudiness on a Global Terrestrial Grid, International Institute for Applied Systems Analyses, Laxenberg, Austria, 62 pp., 1991.

Leuenberger, M., Siegenthaler, U., and Langway, C. C.: Carbon isotope composition of atmospheric CO_2 during the last ice age from an Antarctic ice core, Nature, 357, 488–490, 1992.

Leyden, B. W.: Guatamalan forest synthesis after Pleistocene aridity, P. Natl. Acad. Sci. USA, 81, 4856–4859, 1984.

Leyden, B. W., Brenner, M., Hoddell, D. A., and Curtis, J. H.: Late Pleistocene climate in the central American lowlands, in: American Geophysical Union Geophys. Mono., edited by: Swar, P. K., American Geophysical Union (AGU), Washington D.C., Vol. 78, 1993.

Terrestrial biosphere changes and their impact on ocean δ^{13}C

B. A. A. Hoogakker et al.

Title Page

Abstract	Introduction
Conclusions	References
Tables	Figures

◄◄   ►►

◄   ►

Back   Close

Full Screen / Esc

Printer-friendly Version

Interactive Discussion

Leyden, B. W., Brenner, M., Hodell, D. A., and Curtis, J. H.: Orbital and internal forcing of the climate on the Yucatán peninsula for the past ca. 36 ka, Palaeogeogr. Palaeoclim. Paleoecol., 109, 193–210, 1994.

Lloyd, J. and Farquhar, G. D.: ^{13}C discrimination during CO_2 assimilation by the terrestrial biosphere, Oecologia, 99, 201–215, 1994.

Loulergue, L., Schilt, A., Spahni, R., Masson-Delmotte, V., Blunier, T., Lemieux, B., Barnola, J.-M., Raynaud, D., Stocker, T. F., and Chappellaz, J.: Orbital and millennial-scale features of atmospheric CH_4 over the past 800,000 years, Nature, 453, 383–386, 2008.

Lourantou, A., Lavrič, J. V., Köhler, P., Barnola, J.-M., Paillard, D., Michel, E., Raynaud, D., and Chappellaz, J.: Constraint of the CO_2 rise by new atmospheric carbon isotopic measurements during the last deglaciation, Global Biogeochem. Cy., 24, GB2015, doi:10.1029/2009GB003545, 2010.

Lozano-Garcia, M. S., Ortega-Guerrero, B., and Sosa-Nájera, S.: Mid- to Late-Wisconsin pollen record of San Felipe Basin, Baja California, Quaternary Res., 58, 84–92, 2002.

Magri, D.: Late Quaternary vegetation history at Lagaccione near Lago di Bolsena (central Italy), Rev. Palaeobot. Palyno., 106, 171–208, 1999.

Magri, D. and Sadori, L.: Late Pleistocene and Holocene pollen stratigraphy at Lago di Vico, central Italy, Veg. Hist. Archaeobot., 8, 247–260, 1999.

Magri, D. and Tzedakis, P. C.: Orbital signatures and long-term vegetation patterns in the Mediterranean, Quatern. Int., 73–74, 69–78, 2000.

Marchant, R., Taylor, D., and Hamilton, A.: Late Pleistocene and Holocene history at Mubwindi Swamp, Southwest Uganda, Quaternary Res., 47, 316–328, 1997.

Marchant, R., Cleef, A., Harrison, S. P., Hooghiemstra, H., Markgraf, V., van Boxel, J., Ager, T., Almeida, L., Anderson, R., Baied, C., Behling, H., Berrio, J. C., Burbridge, R., Björck, S., Byrne, R., Bush, M., Duivenvoorden, J., Flenley, J., De Oliveira, P., van Geel, B., Graf, K., Gosling, W. D., Harbele, S., van der Hammen, T., Hansen, B., Horn, S., Kuhry, P., Ledru, M.-P., Mayle, F., Leyden, B., Lozano-García, S., Melief, A. M., Moreno, P., Moar, N. T., Prieto, A., van Reenen, G., Salgado-Labouriau, M., Schäbitz, F., Schreve-Brinkman, E. J., and Wille, M.: Pollen-based biome reconstructions for Latin America at 0, 6000 and 18 000 radiocarbon years ago, Clim. Past, 5, 725–767, doi:10.5194/cp-5-725-2009, 2009.

Martinsen, D. G., Pisias, N. G., Hays, J. D., Imbrie, J., Moore Jr., T. C., and Shackleton, N. J.: Age dating and orbital theory of the ice ages: development of a high resolution 0–300,000 year chronostratigraphy, Quaternary Res., 27, 1–30, 1987.

Terrestrial biosphere changes and their impact on ocean δ^{13}C

B. A. A. Hoogakker et al.

Müller, U. C.: A Late-Pleistocene pollen sequence from the Jammertal, southwestern Germany with particular reference to location and altitude as factors determining Eemian forest composition, Veg. Hist. Archaeobot., 9, 125–131, 2000.

Müller U. C., Pross, J., and Bibus, E.: Vegetation response to rapid climate change in Central Europe during the past 140,000 yr based on evidence from the Füramoos pollen record, Quaternary Res., 59, 235–245, 2003.

Nakagawa, T., Okuda, M., Yonenobu, H., Miyoshi, N., Fujiki, T., Gotanda, K., Tarasov, P., Morita, Y., Takemura, K., and Horie, S.: Regulation of the monsoon climate by two different orbital rhythms and forcing mechanisms, Geology, 36, 491–494, 2008.

Nemani, R. R., Keeling, C. D., Hashimoto, H., Jolly, W. M., Piper, S. C., Tucker, C. K., Myneni, R. B., and Running, S. W.: Climate-driven increases in global terrestrial net primary production from 1982 to 1999, Science, 300, 1560–1563, 2003.

Novenko, E. Y., Seifert-Eulen, M., Boettger, T., and Junge, F. W.: Eemian and Early Weichselian vegetation and climate history in Central Europe: a case study from the Klinge section (Lusatia, eastern Germany), Rev. Palaeobot. Palyno., 151, 72–78, 2008.

Oliver, K. I. C., Hoogakker, B. A. A., Crowhurst, S., Henderson, G. M., Rickaby, R. E. M., Edwards, N. R., and Elderfield, H.: A synthesis of marine sediment core δ^{13}C data over the last 150 000 years, Clim. Past, 6, 645–673, doi:10.5194/cp-6-645-2010, 2010.

Olson, J. S., Watts, J. A., and Allison, L. J.: Carbon in live vegetation of Major world ecosystems, ORNL-5862, National Laboratory, Oak Ridge, Tenessee, 1983.

Parrenin, F., Barnola, J.-M., Beer, J., Blunier, T., Castellano, E., Chappellaz, J., Dreyfus, G., Fischer, H., Fujita, S., Jouzel, J., Kawamura, K., Lemieux-Dudon, B., Loulergue, L., Masson-Delmotte, V., Narcisi, B., Petit, J.-R., Raisbeck, G., Raynaud, D., Ruth, U., Schwander, J., Severi, M., Spahni, R., Steffensen, J. P., Svensson, A., Udisti, R., Waelbroeck, C., and Wolff, E.: The EDC3 chronology for the EPICA Dome C ice core, Clim. Past, 3, 485–497, doi:10.5194/cp-3-485-2007, 2007.

Partridge, T. C., Kerr, S. J., Metcalfe, S. E., Scott, L., Talma, A. S., and Vogel, J. C.: The Pretoria Saltpan: a 200,000 year Southern African lacustrine sequence, Palaeogeogr. Palaeoclim. Paleoecolim. Paleoecol., 101, 317–337, 1993.

Peltier, W. R.: Global glacial isostasy and the surface of the iceage Earth: the ICE-5G (VM2) model and GRACE, Annu. Rev. Earth Pl. Sc., 32, 111–149, 2004.

Penny, D.: A 40,000 palynological record from north-east Thailand: implications for biogeography and palaeo-environmental reconstructions, Palaeogeogr. Palaeoclim. Paleoecol., 171, 97–128, 2001.

Petit, J. R., Jouzel, J., Raynaud, D., Barkov, N. I., Barnola, J.-M., Basile, I., Bender, M., Chappellaz, J., Davis, J., Delaygue, G., Delmotte, M., Kotlyakov, V. M., Legrand, M., Lipenkov, V., Lorius, C., Pepin, L., Ritz, C., Saltzman, E., and Stievenard, M.: Climate and atmospheric history of the past 420 000 years from the Vostok Ice Core, Antarctica, Nature, 399, 429–436, 1999.

Pickett, E., Harrison, S. P., Hope, G., Harle, K., Dodson, J., Kershaw, A. P., Prentice, I. C., Backhouse, J., Colhoun, E. A., D'Costa, D., Flenley, J., Grindrod, J., Haberle, S., Hassell, C., Kenyon, C., Macphail, M., Helene Martin, H., Martin, A. H., McKenzie, M., Newsome, J. C., Penny, D., Powell, J., Raine, J. I., Southern, W., Stevenson, J., Sutra, J.-P., Thomas, I., van der Kaars, S., and War, J.: Pollen-based reconstructions of biome distributions for Australia, Southeast Asia and the Pacific (SEAPAC region) at 0, 6000 and 18,000 ^{14}C yr BP, J. Biogeogr., 31, 1381–1444, 2004.

Piotrowski, A. M., Banakar, V. K., Scrivner, A. E., Elderfield, H., Galy, A., and Dennis, A.: Indian Ocean circulation and productivity during the last glacial cycle, Earth Planet. Sc. Lett., 285, 179–189, 2009.

Pope, V. D., Gallani, M. L., Rowntree, P. R., and Stratton, R. A.: The impact of new physical parameterisations in the Hadley Centre climate model: HadAM3, Clim. Dynam., 16, 123–146, 2000.

Prentice, I. C. and Harrison, S. P.: Ecosystem effects of CO_2 concentration: evidence from past climates, Clim. Past, 5, 297–307, doi:10.5194/cp-5-297-2009, 2009.

Prentice, I. C., Cramer, W., Harrison, S. P., Leemans, R., Monserud, R. A., and Solomon, A. M.: A global biome model based on plant physiology and dominance, soil properties and climate, J. Biogeogr., 19, 117–134, 1992.

Prentice, I. C., Farquhar, G. D., Fasham, M. J. R., Goulden, M. L., Heimann, M., Jaramillo, V. J., Kheshgi, H. S., Le Quéré, C., Scholes, R. J., and Wallace D. W. R.: The carbon cycle and atmospheric carbon dioxide, in: Climate Change 2001: The Scientific Basis. Contribution of Working Group I to the Third Assessment Report of the Intergovernmental Panel on Climate Change, edited by: Houghton, J. T., Ding, Y., Griggs, D. J., Noguer, M., van der Linden, P. J. Dai, X., Maskell, K., and Johnson, C. A., Cambridge University Press, Cambridge, United Kingdom and New York, NY, USA, 881 pp., 2001.

Title Page

Abstract | Introduction

Conclusions | References

Tables | Figures

◄ | ►

◄ | ►

Back | Close

Full Screen / Esc

Printer-friendly Version

Interactive Discussion

Prentice, I. C., Harrison, S. P., and Bartlein, P. J.: Global vegetation and terrestrial carbon cycle changes after the last ice age, New Phytol., 189, 988–998, 2011.

Rickaby, R. E. M., Bard, E., Sonzogni, C., Rostek, F., Beaufort, L., Barker, S., Rees, G., and Schrag, D. P.: Coccolith chemistry reveals secular variations in the global carbon cycle?, Earth Planet. Sc. Lett., 253, 83–95, 2007.

Schmitt, J., Schneider, R., Elsig, J., Leuenberger, D., Lourantou, A., Chappellaz, J., Köhler, P., Joos, F., Stocker, T. F., Leuenberger, M., and Fischer, H.: Carbon isotope constraints on the deglacial CO_2 rise from ice cores, Science, 336, 711–714, 2012.

Scott, L.: The Pretoria Saltpan: a unique source of Quaternary palaeoenvironmental information, S. Afr. J. Sci., 84, 560–562, 1988.

Scott, L.: Palynological analysis of the Pretoria Saltpan (Tswaing crater) sediments and vegetation history in the Bushveld Savanna biome, South Africa, in: Tswaing, Investigations into the Origin, Age and Palaeoenvironments of the Pretoria Saltpan, edited by: Partridge, T. C., Council of Geoscience (Geological Survey of South Africa), Pretoria, 198 pp., 1999a.

Scott, L: Vegetation history and climate in the Savanna biome South Africa since 190,000 ka: a comparison of pollen data from the Tswaing Crater (the Pretoria Saltpan) and Wonderkrater, Quatern. Int., 57–58, 215–223, 1999b.

Shackleton, N. J.: Carbon-13 in Uvigerina: tropical rainforest history and the equatorial Pacific carbonate dissolution cycles, in: The Fate of Fossil Fuel CO_2 in the Oceans, edited by: Anderson, N. and Malahof, A., Plenum, New York, 401–427, 1977.

Sigman, D. M. and Boyle, E. A.: Glacial/interglacial variations in atmospheric carbon dioxide, Nature, 407, 859–869, 2000.

Singarayer, J. S. and Valdes, P. J.: High-latitude climate sensitivity to ice-sheet forcing over the last 120 kyr, Quaternary Sci. Rev., 29, 43–55, 2010.

Smith, R. S.: The FAMOUS climate model (versions XFXWB and XFHCC): description update to version XDBUA, Geosci. Model Dev., 5, 269–276, doi:10.5194/gmd-5-269-2012, 2012.

Smith, R. S. and Gregory, J. M.: The last glacial cycle: transient simulations with an AOGCM, Clim. Dynam., 38, 1545–1559, 2012.

Spahni, R., Chappellaz, J., Stocker, T. F., Loulergue, L., Hausammann, G., Kawamura, K., Fluckiger, J., Schwander, J., Raynaud, D., Masson-Delmotte, V., and Jouzel, J.: Variations of atmospheric methane and nitrous oxide during the last 650000 years from Antarctic ice cores, Science, 310, 1317–1321, 2005.

Stevenson, J. and Hope, G.: A comparison of late Quaternary forest changes in new Caledonia and northeastern Australia, Quaternary Res., 64, 372–383, 2005.

Sykes, C. M. T., Lautenschlager, M., Harrison, S. P., Denissenko, O., and Bartlein, P. J.: Modelling global vegetation patterns and terrestrial carbon storage at the Last Glacial Maximum, Global Ecol. Biogeogr., 3, 67–76, 1993.

Tagliabue, A., Bopp, L., Roche, D. M., Bouttes, N., Dutay, J.-C., Alkama, R., Kageyama, M., Michel, E., and Paillard, D.: Quantifying the roles of ocean circulation and biogeochemistry in governing ocean carbon-13 and atmospheric carbon dioxide at the last glacial maximum, Clim. Past, 5, 695–706, doi:10.5194/cp-5-695-2009, 2009.

Takahara, H., Sugita, S., Harrison, S. P., Miyoshi, N., Morita, Y., and Uchiyama., T.: Pollen-based reconstructions of Japanese biomes at 0, 6000 and 18,000 ^{14}C yr BP, J. Biogeogr., 27, 665–683, 1999.

Tarasov, P. E., Webb, T., Andreev, A. A., Afanas'eva, N. B., Berezina, N., Bezusko, L. G., Blyaharchuk, T. A., Bolikhovskaya, N. S., Cheddadi, R., Chernavskaya, M. M., Chernova, G. M., Dorofeyuk, N. I., Dirksen, V. G., Elina, G. A., Filminova, L. V., Glebov, F. Z., Guiot, J., Gunova, V. S., Harrison, S. P., Jolly, D., Khomutova, V. I., Kvavadze, E. V., Osipova, I. M., Panova. N. K., Prentice, I. C., Saarse, L., Sevastyanov, D. V., Volkova, V. S., and Zernitskaya, V. P.: Present-day and mid-Holocene biomes reconstructed from pollen and plant marcofossil data from the former Soviet Union and Mongolia, J. Biogeogr., 25, 1029–1053, 1998.

Tarasov, P. E., Volkova, V. S., Webb, T., Guiot, J., Andreev, A. A., Bezusko, L. G., Bezusko, T. V., Bykova, G. V., Dorofeyuk, N. I., Kvavadze, E. V., Osipova, I. M., Panova, N. K., and Sevastyanov, D. V.: Last Glacial Maximum biomes reconstructed from pollen and plant macrofossil data from Northern Eurasia, J. Biogeogr., 27, 609–620, 2000.

Thompson, R. S. and Anderson, K. H.: Biomes of Western North America at 18,000, 6000 and 0 ^{14}C yr BP reconstructed from pollen and packrat midden data, J. Biogeogr., 27, 555–584, 2000.

Timm, O. and Timmermann, A.: Simulation of the last 21,000 years using accelerated transient boundary conditions, J. Climate, 20, 4377–4401, 2007.

Tinker, P. B. and Ineson, P.: Soil organic matter and biology in relation to climate change, In: Soils on a Warmer Earth, Developments in Soil Science, edited by: Scharpenseel, H. W., Schomaker, M., and Ayoub, A., Vol. 20, Elsevier, Amsterdam, 71–87, 1990.

Title Page

Abstract | Introduction

Conclusions | References

Tables | Figures

◄◄ | ►►

◄ | ►

Back | Close

Full Screen / Esc

Printer-friendly Version

Interactive Discussion

Tzedakis, P. C., Frogley, M. R., and Heaton, T. H. E.: Duration of last interglacial in northwestern Greece, Quaternary Res., 58, 53–55, 2002.

Tzedakis, P. C., Frogley, M. R., Lawson, I. T., Preece, R. C., Cacho, I., and de Abreu, L.: Ecological thresholds and patterns of millennial-scale climate variability: the response of vegetation in Greece during the last glacial period, Geology, 32, 109–112, 2004a.

Tzedakis, P. C., Roucoux, K. H., De Abreu, L., and Shackleton, N. J.: The duration of forest stages in southern Europe and interglacial climate variability, Science, 3006, 2231–2235, 2004b.

Tzedakis, P. C., Hooghiemstra, H., and Pälike, H.: The last 1.35 million years at Tenaghi Philippon: revised chronostratigraphy and long-term vegetation trends, Quaternary Sci. Rev., 23–24, 3416–3430, 2006.

van der Hammen, T. and González, E.: Upper Pleistocene and Holocene climate and vegetation of the Saban de Bogotá, Leides Geologische Mededelingen, 25, 261–315, 1960.

Vandergoes, M. J., Newnham, R. M., Preusser, F., Hendy, C. H., Lowell, T. V., Fitzsimons, S. J., Hogg, A. G., Kasper, H. U., and Schlüchter, C.: Regional insolation forcing of late Quaternary climate change in the Southern Hemisphere, Nature, 436, 242–245, 2005.

Velichko, A. A., Novenko, E. Y., Pisareva, V. V., Zelikson, E. M., Boettger, T., and Junge, F. W.: Vegetation and climate changes during the Eemian interglacial in Central and Eastern Europe: comparative analysis of pollen data, Boreas, 34, 207–219, 2005.

Voelker, A. H. L. and workshop participants: Global distribution of centennial-scale records for Marine Isotope Stage (MIS) 3: a database, Quaternary Sci. Rev., 21, 1185–1212, 2002.

Wang, P., Tian, J., Cheng, X., Liu, C., and Xu, J.: Carbon reservoir changes preceded major ice-sheet expansion at the mid-Brunhes event, Geology, 31, 239–242, 2003.

Wang, Y., Cheng, H., Edwards, R. L., Kong, X., Shao, X., Chen, S., Wu, J., Jiang, X., Wang, X., and An, Z.: Millennial-and orbital-scale changes in the East Asian monsoon over the past 224,000 years, Nature, 451, 1090–1093, 2008.

Watts, W. A. and Bradbury, J. P.: Palaeoecological studies on Lake Patzcuaro on the west-central Mexican Plateau and at Chalco in the Basin of México, Quaternary Res., 17, 56–70, 1982.

Whitlock, C. and Bartlein, P. J.: Vegetation and climate change in northwest America during the past 125 kyr, Nature, 388, 57–61, 1997.

Wijmstra, T. A.: Palynology of the first 30 m of a 120 m deep section in northern Greece, Acta Bot. Neerl., 18, 511–527, 1969.

Wijmstra, T. A. and Smith, A.: Palynology of the middle part (30–78 metres) of a 120 m deep section in northern Greece (Macedonia), Acta Bot. Neerl., 25, 297–312, 1976.

Williams, J. W., Webb, T., Richard, P. H., and Newby, P.: Late Quaternary biomes of Canada and the eastern United States, J. Biogeogr., 27, 585–607, 2000.

5 Zinke, P. J., Stangenberger, A. G., Post, W. M., Emanuel, W. R., and Olson, J. S.: Worldwide organic soil carbon and nitrogen data, ORNLITM8857, Oak Ridge National Laboratory Oak Ridge, 1984.

Terrestrial biosphere changes and their impact on ocean δ^{13}C

B. A. A. Hoogakker et al.

Table 1. Details of the various biomization schemes applied for the different regions.

Africa	Jolly et al. (1998)
Southeast Asia, Australia	Pickett et al. (2004)
Japan	Takahara et al. (1999)
Southern Europe	Elenga et al. (2000)
North East Europe	Tarasov et al. (2000)
North America: Western North	Thompson and Anderson (2000)
North America: East and North East	Williams et al. (2000)
Latin America	Marchant et al. (2009)

Table 2. Details of the locations of pollen-data records synthesised in this study.

	Core	Latitude	Longitude	A.S.L. (m)	Age ~ (ka BP)	Reference	Biomization reference
North America							
Canada (short)	Brother-of-Fog	67.18	−63.25	380	Last interglacial	Frechette et al. (2006)	Williams et al. (2000)
Canada (short)	Amarok	66.27	−65.75	848	Holocene and last interglacial	Frechette et al. (2006)	Williams et al. (2000)
USA	Carp Lake	45.92	−120.88	714	0 to ca 130	Whitlock and Bartlein (1997)	Thompson and Anderson (2000)
USA	Bear Lake	41.95	−111.31	1805	0 to 150	Jiménez-Moreno et al. (2007)	Thompson and Anderson (2000)
USA	Potato lake	34.4	−111.3	2222	2 to ca 35	Anderson et al. (1993)	Thompson and Anderson (2000)
USA	San Felipe	31	−115.25	400	16 to 42	Lozano-Garcia et al. (2002)	Thompson and Anderson (2000)
USA	Lake Tulane	27.59	−81.50	36	0 to 52	Grimm et al. (2006)	Williams et al. (2000)
Latin America							
Mexico	Lake Patzcuaro	19.58	−101.58	2044	3 to 44	Watts and Bradbury (1982)	Marchant et al. (2009)
Guatamala	Lake Petén-Itzá	16.92	−89.83	110	0–86	Correa-Metrio et al. (2012)	Marchant et al. (2009)
Colombia	Ciudad Universitaria X	−4.75	−74.18	2560	0 to 35	van der Hammen and González (1960)	Marchant et al. (2009)
Peru	Laguna Junin	−11.00	−76.18	4100	0 to 36 (LAPD1?)	Hansen et al. (1984)	Marchant et al. (2009)
Peru/Bolivia	Lake Titicaca	−15.9	−69.10	3810	3–370 (shown until 140)	Gosling et al. (2008); Hanselman et al. (2011); Fritz et al. (2007)	Marchant et al. (2009)
Guatamala	Lago Quexil	16.92	−89.88	110	9 to 36	Leyden (1984); Leyden et al. (1993, 1994)	Marchant et al. (2009)
Brazil	Salitre	−19.00	−46.77	970	2 to 50 (LAPD1)	Ledru (1992, 1993); Ledru et al. (1994, 1996)	Marchant et al. (2009)
Brazil	Colonia	−23.87	−46.71	900	0 to 120	Ledru et al. (2009)	Marchant et al. (2009)
Brazil	Cambara	−29.05	−50.10	1040	0 to 38	Behling et al. (2004)	Marchant et al. (2009)
Peru/Bolivia	Lake Titicaca	~ −16 to −17.5	~ −68.5 to −70	3810	3–138	Hanselman et al. (2011); Fritz et al. (2007)	Marchant et al. (2009)
Bolivia	Uyuni	−20.00	−68.00	653	17 to 108	Chepstow Lusty et al. (2005)	Marchant et al. (2009)

Table 2. Continued.

	Core	Latitude	Longitude	A.S.L. (m)	Age ~ (ka BP)	Reference	Biomization reference
Europe							
Russia	Butovka	55.17	36.42	198	Holocene, early glacial and Eemian	Borisova (2005)	Tarasov et al. (2000)
Russia	Ilinskoye	53	37	167	early glacial and Eemian	Grichuk et al. (1983); Velichko et al. (2005)	Tarasov et al. (2000)
Poland	Horoszki Duze	52.27	23		~ 75 to Eemian		Tarasov et al. (2000)
Germany	Klinge	51.75	14.51	80	early glacial, Eemian and Saalian (penultimate glacial)	Novenko et al. (2008)	Tarasov et al. (2000)
Germany	Füramoos	47.59	9.53	662	0 to 120	Muller et al. (2003)	Prentice et al. (1992)
Germany	Jammertal	48.10	9.73	578	Eemian	Muller (2000)	Prentice et al. (1992)
Germany	Samerberg	47.75	12.2	595	Eemian and early Würmian	Grüger (1979a, b)	Prentice et al. (1992)
Germany	Wurzach	47.93	9.89	650	Eemian and early Würmian	Grüger and Schreiner (1993)	Prentice et al. (1992)
Italy	Lagaccione	42.57	11.85	355	0 to 100	Magri (1999)	Elenga et al. (2004)
Italy	Lago di Vico	42.32	12.17	510	0 to 90	Magri and Sadori (1999)	Elenga et al. (2004)
Italy	Valle di Castiglione	41.89	12.75	44	0 to 120	Magri and Tzedakis (2000)	Elenga et al. (2004)
Italy	Monticchio	40.94	15.60	656	0 to 120	Allen et al. (1999)	Elenga et al. (2004)
Greece	Ioannina	39.76	20.73	470	0 to 120	Tzedakis et al. (2002, 2004a)	Elenga et al. (2004)
Greece	Tenaghi Philippon	41.17	24.30	40	0 to 120	Wijmstra (1969); Wijmstra and Smith (1976); Tzedakis et al. (2006)	Elenga et al. (2004)
Africa							
Uganda	ALBERT-F	1.52	30.57	619	0 to 30	Beuning et al. (1997)	Jolly et al. (1998)
Uganda	Mubwindi swamp3	−1.08	29.46	2150	0 to 40	Marchant et al. (1997)	Jolly et al. (1998)
Rwanda	Kamiranzovy swamp 1	−2.47	29.12	1950	13 to 40	Bonnefille and Chalie (2000)	Jolly et al. (1998)
Burundi	Rusaka	−3.43	29.61	2070	0 to 47	Bonnefille and Chalie (2000)	Jolly et al. (1998)
Burundi	Kashiru Swamp A1	−3.45	29.53	2240	0 to 40	Bonnefille and Chalie (2000)	Jolly et al. (1998)
Burundi	Kashiru Swamp A3	−3.45	29.53	2240	0 to 40	Bonnefille and Chalie (2000)	Jolly et al. (1998)
Tanzania	Uluguru	−7.08	37.62	2600	0 to > 45	Finch et al. (2009)	Jolly et al. (1998)
Madagascar	Lake Tritrivakely	−19.78	46.92	1778	0 to 40	Gasse and Van Campo (1998)	Jolly et al. (1998)
South Africa	Tswaing (Saltpan) Crater	−25.57	28.07	1100	0 to 120 (although after 35 probably less secure based)	Scott (1988b); Partridge et al. (1993); Scott (1999a, b)	Jolly et al. (1998)
South Africa	Mfabeni swamp	−28.13	32.52	11	0 to 43	Finch and Hill (2008)	Jolly et al. (1998)

Title Page

Abstract | Introduction

Conclusions | References

Tables | Figures

◄◄ | ►►

◄ | ►

Back | Close

Full Screen / Esc
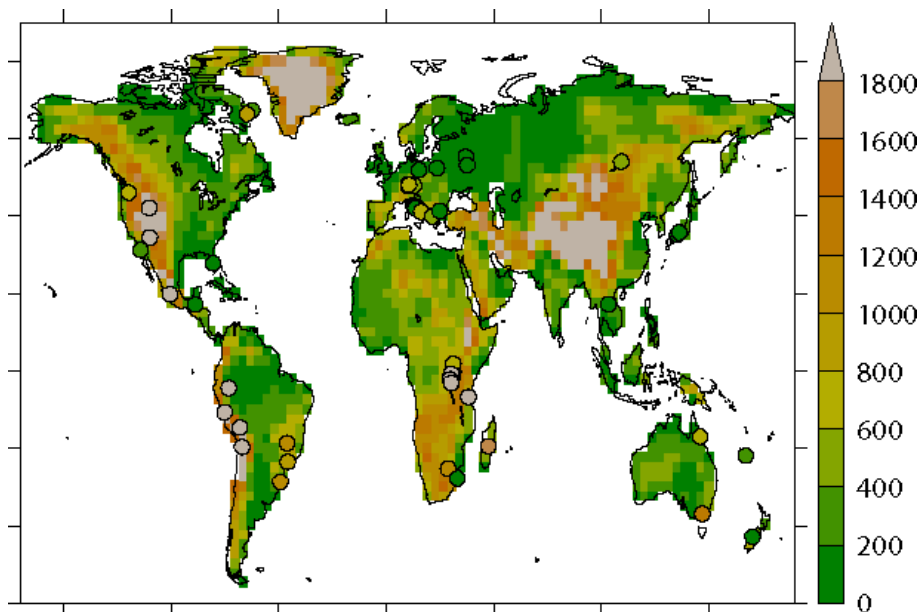
Printer-friendly Version

Interactive Discussion

Discussion Paper | Discussion Paper | Discussion Paper | Discussion Paper

CPD

11, 1031–1091, 2015

Terrestrial biosphere changes and their impact on ocean δ^{13}C

B. A. A. Hoogakker et al.

Title Page

Abstract | Introduction

Conclusions | References

Tables | Figures

|◄ | ►|

◄ | ►

Back | Close

Full Screen / Esc

Printer-friendly Version

Interactive Discussion

Table 2. Continued.

	Core	Latitude	Longitude	A.S.L. (m)	Age ~ (ka BP)	Reference	Biomization reference
Australasia							
Russia	Lake Baikal	53.95	108.9		114–130	–	–
Japan	Lake Biwa	35	135	85.6	0–120	Nakagawa et al. (2008)	Takahara et al. (1999)
Japan	Lake Suigetsu	35.58	135.88	∼ 0	0–120	Nakagawa (2008)	Takahara et al. (1999)
Thailand	Khorat Plateau	17	103	∼ 180	0–40	Penny (2001)	Pickett et al. (2004)
Australia	Lynch's Crater	−17.37	145.7	760	0–120	Kershaw (1986)	Pickett et al. (2004)
New Caledonia	Xero Wapo	−22.28	166.97	220	0–120	Stevenson and Hope (2005)	Pickett et al. (2004)
Australia	Caldeonia fen	−37.33	146.73	1280	0–120	Kershaw et al. (2007)	Pickett et al. (2004)
New Zealand	Okarito	−43.24	170.22	70	0–120	Vandergoes et al. (2005)	Pickett et al. (2004)

Figure 1. Locations and altitudes of pollen records superimposed on pre-industrial HadCM3 orography (m).
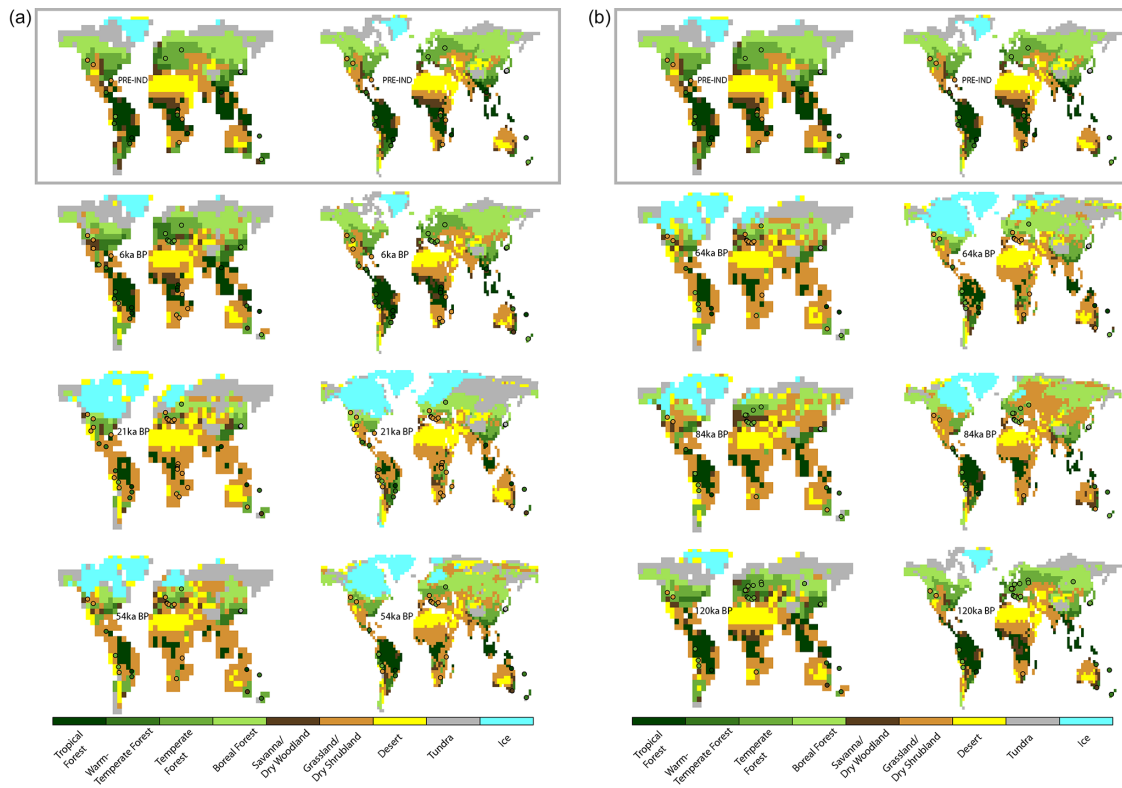
Figure 2. Biome reconstructions from FAMOUS and HadCM3 climates for selected marine isotope stages (denoted in ka BP). The biome with the highest affinity score for each site in our synthesis where there is pollen during this stage is superimposed.

Title Page

Abstract | Introduction

Conclusions | References

Tables | Figures

◄ | ►

◄ | ►

Back | Close

Full Screen / Esc

Printer-friendly Version

Interactive Discussion
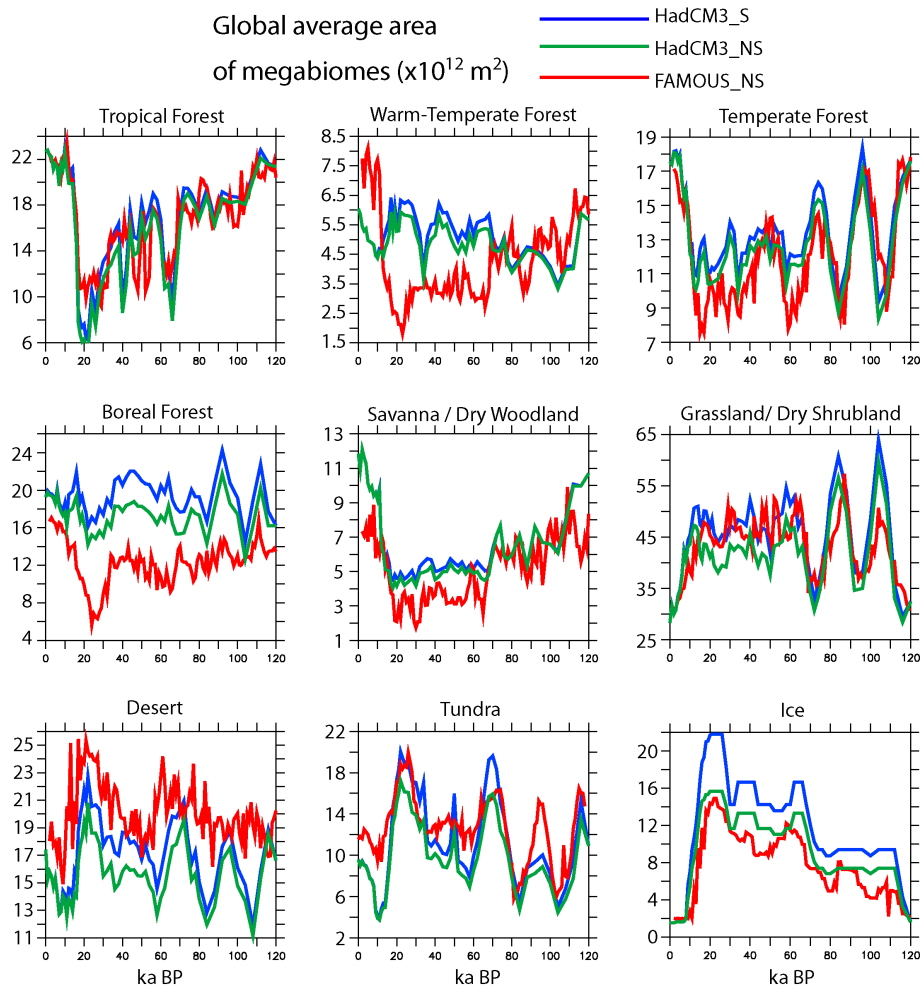
Figure 3. Global area coverage of megabiome types in the model reconstructions.

Title Page

Abstract | Introduction

Conclusions | References

Tables | Figures

|◄ | ►|

◄ | ►

Back | Close

Full Screen / Esc

Printer-friendly Version

Interactive Discussion

Full Screen / Esc

Printer-friendly Version

Interactive Discussion
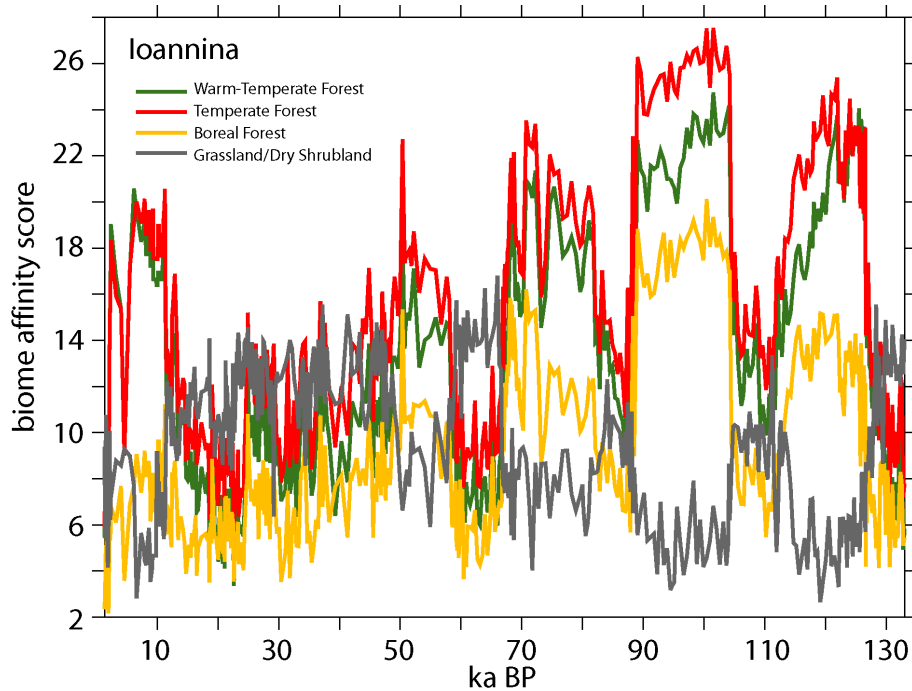
Figure 4. Affinity scores for the 4 dominant biome types at the Ioannina site (20.73° E, 39.76° N) from Greece.
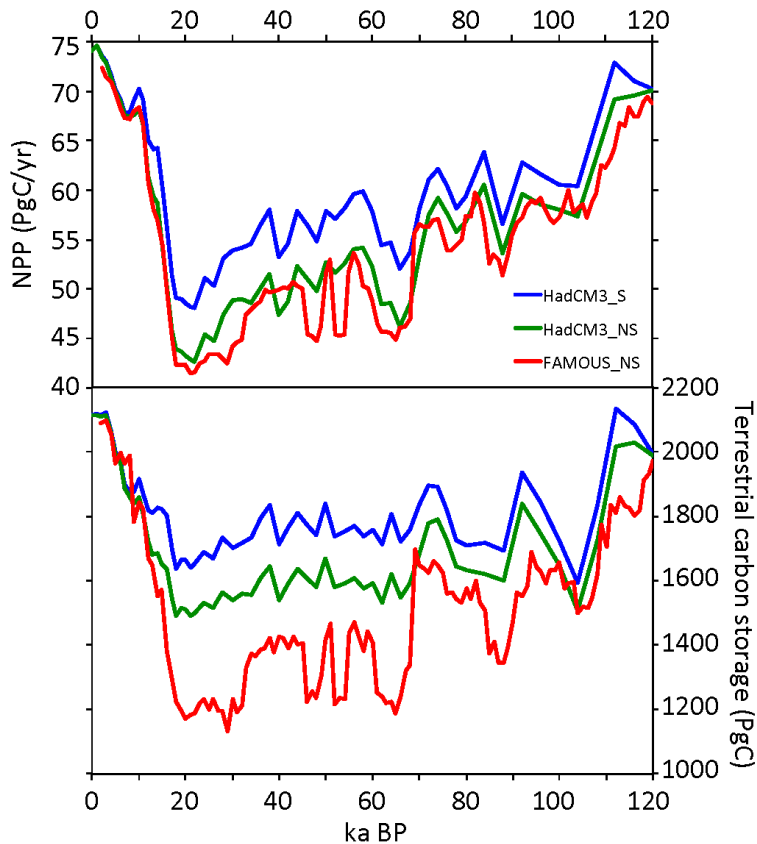
Figure 5. Net Primary Production and carbon storage throughout the last glacial cycle derived from the model-based biome reconstructions. HadCM3_S includes the additional influence of land exposed by sea-level changes, HadCM3_NS and FAMOUS_NS do not.

Title Page

Abstract   Introduction

Conclusions   References

Tables   Figures

|◄   ►|

◄   ►

Back   Close

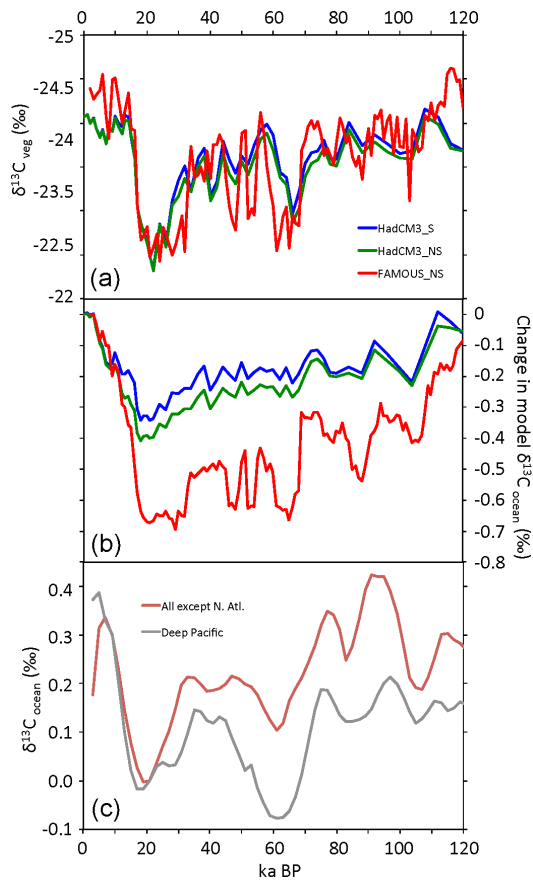Full Screen / Esc

Printer-friendly Version

Interactive Discussion

Figure 6. (a) Modelled $\delta^{13}C$ for terrestrial biosphere; **(b)** change in modelled total ocean $\delta^{13}C$, **(c)** benthic foraminifera deep ocean $\delta^{13}C$ compiled by Oliver et al. (2010).

Title Page

Abstract · Introduction

Conclusions · References

Tables · Figures

◀ · ▶

◀ · ▶

Back · Close

Full Screen / Esc

Printer-friendly Version

Interactive Discussion